

# JGR Atmospheres

## RESEARCH ARTICLE

10.1029/2020JD033659

### Key Points:

- Default parameter values in Noah-MP lead to underestimation of latent heat fluxes and overestimation of soil moisture
- The introduction of lateral flow via Weather Research and Forecasting-Hydro can alleviate the biases in latent heat fluxes in high-resolution simulations
- It is crucial to address parametric uncertainty in both land surface and routing schemes for realistic surface flux simulations

### Supporting Information:

Supporting Information may be found in the online version of this article.

### Correspondence to:

Z. Yang and L. Berg,  
[Zhao.Yang@pnnl.gov](mailto:Zhao.Yang@pnnl.gov);  
[Larry.Berg@pnnl.gov](mailto:Larry.Berg@pnnl.gov)

### Citation:

Yang, Z., Huang, M., Berg, L. K., Qian, Y., Gustafson, W. I., Fang, Y., et al. (2021). Impact of lateral flow on surface water and energy budgets over the southern Great Plains—A modeling study. *Journal of Geophysical Research: Atmospheres*, 126, e2020JD033659.  
<https://doi.org/10.1029/2020JD033659>

Received 5 AUG 2020  
Accepted 14 JAN 2021

## Impact of Lateral Flow on Surface Water and Energy Budgets Over the Southern Great Plains—A Modeling Study

Zhao Yang<sup>1</sup> , Maoyi Huang<sup>2</sup> , Larry K. Berg<sup>1</sup> , Yun Qian<sup>1</sup> , William I. Gustafson<sup>1</sup> , Yuanhao Fang<sup>3</sup> , Ying Liu<sup>1</sup> , Jerome D. Fast<sup>1</sup>, Koichi Sakaguchi<sup>1</sup> , and Sheng-Lun Tai<sup>1</sup> 

<sup>1</sup>Pacific Northwest National Laboratory, Richland, WA, USA, <sup>2</sup>Office of Science and Technology Integration, National Weather Service, National Oceanic and Atmospheric Administration, Silver Spring, MD, USA, <sup>3</sup>Department of Hydrology and Atmospheric Sciences, University of Arizona, Tucson, AZ, USA

**Abstract** As the horizontal grid spacing decreases, treatment of hydrologic processes in land surface models (LSMs), such as the lateral flow of surface and subsurface flow, need to be explicitly represented. Unlike previous studies that mainly focused on the mountainous regions, in this study, the offline Weather Research and Forecasting (WRF)-Hydro model is employed to study the impact of lateral flow on soil moisture and energy fluxes over the relatively flat southern Great Plains (SGP). The vast amount of measurements over the SGP provide a unique opportunity to assess the model behavior. In addition, newly developed land surface properties and input forcing are ingested into the model, in an attempt to reduce uncertainties associated with the initial and boundary forcing and help to identify model deficiencies. Our results show that the more realistic inputs (parameters, soil types, forcing) lead to larger underestimation of latent heat flux and dry bias, indicating the existence of model structural uncertainty (embedded errors) in WRF-Hydro that need to be characterized to inform future model development efforts. Including lateral flow processes partly mitigates the model deficiencies in representing hydrologic processes and alleviates the dry bias. In particular, both surface and subsurface lateral flow increase soil moisture mainly over the lower elevations, except that subsurface flow also affects soil moisture over steeper terrains. Additional simulations are performed to assess the effect of routing resolution on model results. When LSM resolution is high, noticeable differences in soil moisture are produced between different routing resolutions especially over steep terrain. Whereas when LSM resolution is coarse, differences between routing resolutions become negligible, especially over flat terrain.

## 1. Introduction

The emerging demand to obtain predictability for terrestrial ecosystems across landscapes, with water, energy, and nutrients as drivers of these dynamic systems, requires process-level understanding at O(1 km) globally, or O(100 m) locally (Wood et al., 2011); this is known as the so-called hyperresolution scale. These hyperresolution simulations would require extensive computation costs, which were previously unrealistic but have become increasingly possible.

The advocacy of hyperresolution land surface models (LSMs) calls for the need to realistically representing hydrologic processes as well as surface hydrologic information such as topography, vegetation, and soil hydraulic parameters (Chaney et al., 2016; Clark et al., 2015; Fan et al., 2019; Maxwell et al., 2015; Wood et al., 2011). Hyperresolution LSMs face the challenge to represent hydrologic processes at the hillslope-to-catchment scales (O(~10 m–10 km)). These hydrologic processes, that is, topographic gradient driven processes, such as water or sediment transport from the ridges to valleys, operate at scales finer than the traditional LSMs (O(10 km)) and need to be considered when LSMs are used at hyperresolution scales.

Several previous attempts have been made to understand the importance of lateral flow due to their importance in hydrologic states and land-atmosphere interactions (Arnault et al., 2016, 2018, 2019; Chaney et al., 2016; Fan et al., 2019; Ji et al., 2017; Lahmers et al., 2019; Maxwell et al., 2015; Rummel et al., 2019; Senatore et al., 2015; Z. Zhang et al., 2019, and references therein). However, these previous studies have primarily focused on the mountainous regions, however it is still unknown if lateral flow is equally important

over the relatively flat southern Great Plains (SGP). Therefore, one goal of this study is to understand how lateral flow would affect soil moisture and surface fluxes over the SGP, where extensive observations are readily available for evaluating model performance (shown later).

Focusing on the effect of lateral surface and subsurface flow, Maxwell et al. (2015) found that the physics-based integrated hydrologic model Parflow can reproduce streamflow and water table depths reasonably well over the majority of the Continental US (CONUS). Chaney et al. (2016) developed HydroBlocks that accounts for spatial heterogeneity through hydrologic response units (HRU). These HRUs are defined using cluster analysis based on land cover, topography, soil, and location. The vertical profiles of each HRU are then updated using the Noah-MP LSM (Niu et al., 2011) and exchanges between HRUs are controlled by the dynamic TOPMODEL via a subsurface kinematic wave. Ji et al. (2017) suggested that surface lateral flow has a significant influence on soil moisture and evapotranspiration (ET) even at coarse resolutions, and subsurface lateral flow causes drier ridgelines and wetter valleys. Arnault et al. (2016) found that overland flow clearly increases infiltration and evapotranspiration at the beginning of the wet season when soil is still dry. Z. Zhang et al. (2019) used the fully coupled Weather Research and Forecasting (WRF) model with its hydrological extension WRF-Hydro (Gochis et al., 2018) and reported a redistribution of infiltration excess in the mountainous area. Such realistic treatments of hydrologic processes in coupled models typically lead to higher soil moisture content in the root zone, increases the terrestrial water storage and evapotranspiration, and decreases the total runoff over the mountainous regions.

It is known that the lateral flow is generally more important at finer grid resolution. Previous studies suggest treating lateral flow at resolutions of 1 km or finer (Gochis & Chen, 2003). This is due to the fact that typical overland flood waves are at length scales smaller than 1 km. At larger scales, flood wave and micro-topography features that affect it are poorly represented. Additionally, at coarser resolutions, terrain slopes between grid cells are smoothed as resolution becomes coarser, which means the lateral flow impact is also scale-dependent. Therefore, the impacts of lateral flow on land surface water and energy budgets differ and are dependent on landscape characteristics of interest, but it is still not clear at what scale the effects of surface and subsurface lateral flows become non-negligible. Therefore, another goal of this study is to examine the critical resolution at which the lateral flow becomes non-negligible with WRF-Hydro over the SGP. To achieve that, we performed sensitivity experiments of different horizontal routing resolution at various LSM resolutions. The outcome of this analysis could serve as guidance for future coupled model experiments.

High-resolution LSMs will entail an unprecedented demand for high-resolution land characterization data (Wood et al., 2011), such as soil properties, land use, and land cover type, and vegetation characteristics. An important source of uncertainty in LSMs lies in inaccuracies in characterizing these land properties. Recently developed remote sensing and field surveys provide additional sources of land characteristic data sets for vegetation or soil types that may not be promptly realized by the modeling community. The utilization of these data sets, assuming they contain less uncertainty than the old data sets, is therefore important for identifying model deficiencies and structural errors and guiding future model development.

The representation of soil and vegetation have been found to be a major source of uncertainty in regional hydrologic simulations (De Lannoy et al., 2014; Livneh et al., 2015; Osborne et al., 2004; Shi et al., 2014). For example, Osborne et al. (2004) found that soil properties could affect the portioning of surface and subsurface runoff by examining the effects of soil texture. Using two different soil data sets, Livneh et al. (2015) reported quite different response to extreme events (floods and droughts). Similarly, the soil hydraulic properties, which are defined depending on the soil texture of a grid cell following a pre-defined soil parameter table (i.e., SOILPARM), are important since they affect water and energy fluxes exchanges within the soil column, and hence water availability for evapotranspiration. These parameters determine the soil hydraulic properties and are obtained through field measurements or parameter estimation. In particular, the default soil parameter table has been developed through the earlier efforts by Cosby et al. (1984), Chen and Dudhia (2001), NCEP (2012), and Peters-Lidard et al. (1998). For detail description of the table, readers may refer to Tables 1 and 2 in Kishn   et al. (2017). These soil hydraulic parameters are applied both during initializing and running the land surface models, therefore have far-reaching influence on the outcomes of land surface states in both the coupled and uncoupled modes (Kishn   et al., 2017). The misrepresentation of vegetation is also a source of uncertainty in the land surface models. Depending on the option chosen,

vegetation dynamics could be treated differently in the land surface models. Kumar et al. (2014) found improvement in surface heat fluxes and surface temperature and moisture when realistic vegetation parameters are incorporated into the model. The realistic implementation of satellite-based leaf-area index (LAI) are also found to reduce temperature biases using different climate models (Boussetta et al., 2013, 2014; Knote et al., 2009). Considering the uncertainties associated with the initial and boundary conditions, the last goal of this study is to evaluate their impacts on soil moisture and surface fluxes, in an attempt to better simulate the soil moisture and energy fluxes. By using the most realistic input forcing as possible, this will help to identify model deficiency and guide future model development.

To summarize, this study will address the following goals related to simulating soil moisture and energy fluxes over the SGP. Using WRF-Hydro, the first goal is to assess the role of input forcings in the default Noah-MP LSM. Routing options are turned off at this stage. The second goal is to understand how surface and subsurface lateral flow would affect soil moisture and energy, respectively. We achieve this by switching on and off the lateral flow options in the WRF-Hydro model. Finally, the third goal is to understand the impact of routing resolution on soil moisture and energy fluxes over the SGP.

## 2. Methods

### 2.1. Model Description

WRF-Hydro was designed as an extensible modeling framework that can host a regional climate model, a land surface model, and a hydrological model. In this study, we focus on evaluating the offline mode of the model system, without coupling a regional climate model, to quantify potential issues in land surface representations. The WRF-Hydro hydrological extension includes a distributed three-dimensional, variably saturated surface and subsurface flow, channel flow, and a bucket model to account for baseflow. The lateral surface and subsurface flow are computed on a separate grid nested within the land surface model grid, which can have a different resolution than the land surface model. The difference in resolution requires a disaggregation-aggregation procedure to map land surface hydrological conditions from a “coarse” land surface model grid to a much more finely resolved terrain routing grid (Gochis & Chen, 2003).

Specifically, the disaggregation process is initiated after the LSM process and prior to the routing of subsurface and surface (Rummel et al., 2019). After the LSM process, the specific hydrologic variables, such as soil moisture content and infiltration excess, are updated by the LSM and divided up from the LSM grid into the subgrid cells. Subsurface lateral flow is calculated prior to the routing of surface flow to allow for exfiltration from fully saturated soil columns to be added to the infiltration excess. The subsurface routing scheme was calculated following the method in Wigmosta et al. (1994) and Wigmosta and Lettenmaier (1999). It calculates a quasi-three-dimensional flow, which includes the effects of topography, saturated soil depth, and saturated hydraulic conductivity. Note that lateral subsurface flow only exists in the saturated soil layers and the hydraulic gradient is calculated based on the slope of the adjacent water table, which is the depth of the top of the highest saturated layer.

Surface flow is achieved using a fully unsteady, explicit, finite-difference, diffusive wave formulation (Julien et al., 1995; Ogden, 1997), which can account for backwater effects and flow on adverse slopes (Senatore et al., 2015). In WRF-Hydro, there are two options available for surface lateral flow, two-dimensional flow that consider  $x$ - and  $y$ -dimensional or one-dimensional flow (“D8”) that water flows along the steepest gradient based on total water head gradient. Overland flow becomes channel inflow if it reaches a channel grid, or it remains as surface runoff. This study utilizes the steepest gradient method for surface flow. Water flows out of the bottom soil layer and will go through a groundwater bucket with a fixed capacity; the baseflow is calculated using an exponential function.

After water is routed through hillslopes along the surface or in the subsurface, through the groundwater aquifer and channels, state variables such as soil moisture and ponded water on the routing grid are aggregated back to the native LSM grid using a simple linear average operator. These updated values are then passed to the next iteration of the LSM timestep.

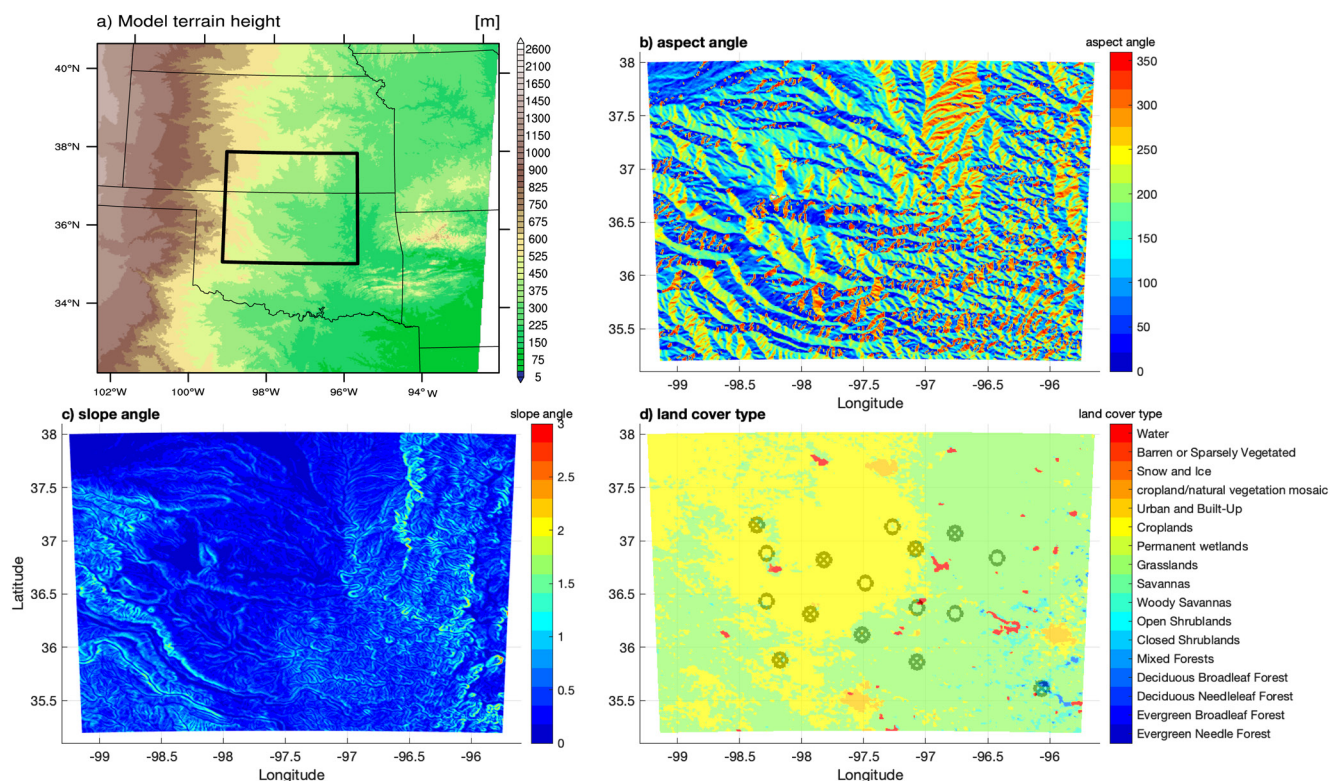


**Figure 1.** General geophysical features within the research domain. (a) Terrain height (units: m) with black box delineating our model domain. (b) Aspect angle, which is defined as the direction in which elevation decreases most rapidly, expressed as an azimuth measured clockwise from north (units: degree). (c) Slope angle, it is the gradient in the direction in which elevation decreases most rapidly (units: degree). (d) Land use and land cover type within the domain. Circles indicate Soil Temperature and Moisture Profiles locations and crosses indicate locations of energy balance Bowen ratio and eddy correlation stations.

## 2.2. Study Area and Observation Data

Our study domain is located over the SGP and covers the spatial extent of  $35.2^{\circ}$ – $38.0^{\circ}$ N and  $95.6^{\circ}$ – $99.2^{\circ}$ W (see Figure 1). The spatial domain covers 392 km in both the zonal and meridional directions. The domain represents a moderate transitional zone with land cover mostly consisting of cropland and grassland moving from east to west (Koster et al., 2004). The domain-wide annual average precipitation is approximately 850 mm according to the PRISM data (Daly et al., 2008). It features relatively flat terrain with generally higher elevations on the order of 2,100 m to the west and lower elevations around 300 m to the east. There are local topographic features with sharp gradients to the southwest of the domain with slopes around 3.5°.

It features extensive observation sites located within the domain, including the US Department of Energy (DOE) Atmospheric Radiation Measurement (ARM) user facility, which contains a number of extended sites, which provide a unique opportunity as reference data sets. Surface energy fluxes are available at the ARM sites, collected by using either the eddy correlation (ECOR) or energy balance Bowen ratio (EBBR) methods (Figure 1d). Soil moisture and soil type data sets are available from the Soil Temperature and Moisture Profiles (STAMP) from the ARM sites (Figure 1d). There are 16 STAMP sites available within the domain. The observation period for STAMP sites begins in late 2015 and, therefore, model simulated soil moisture are compared to STAMP sites for 2016 only due to data availability.

## 2.3. Input and Forcing Data

The National Land Data Assimilation System Phase 2 (NLDAS-2, Xia et al., 2012) is employed to drive the model. NLDAS-2 is available at  $1/8^{\circ}$  grid spacing. The model is simulated from 2008 to 2016, the first 3 years are treated as spin-up period. Year 2011–2015 are used for evaluating latent and sensible heat flux, and 2016 for soil moisture given the availability of observation data sets. Variables used to force the model include

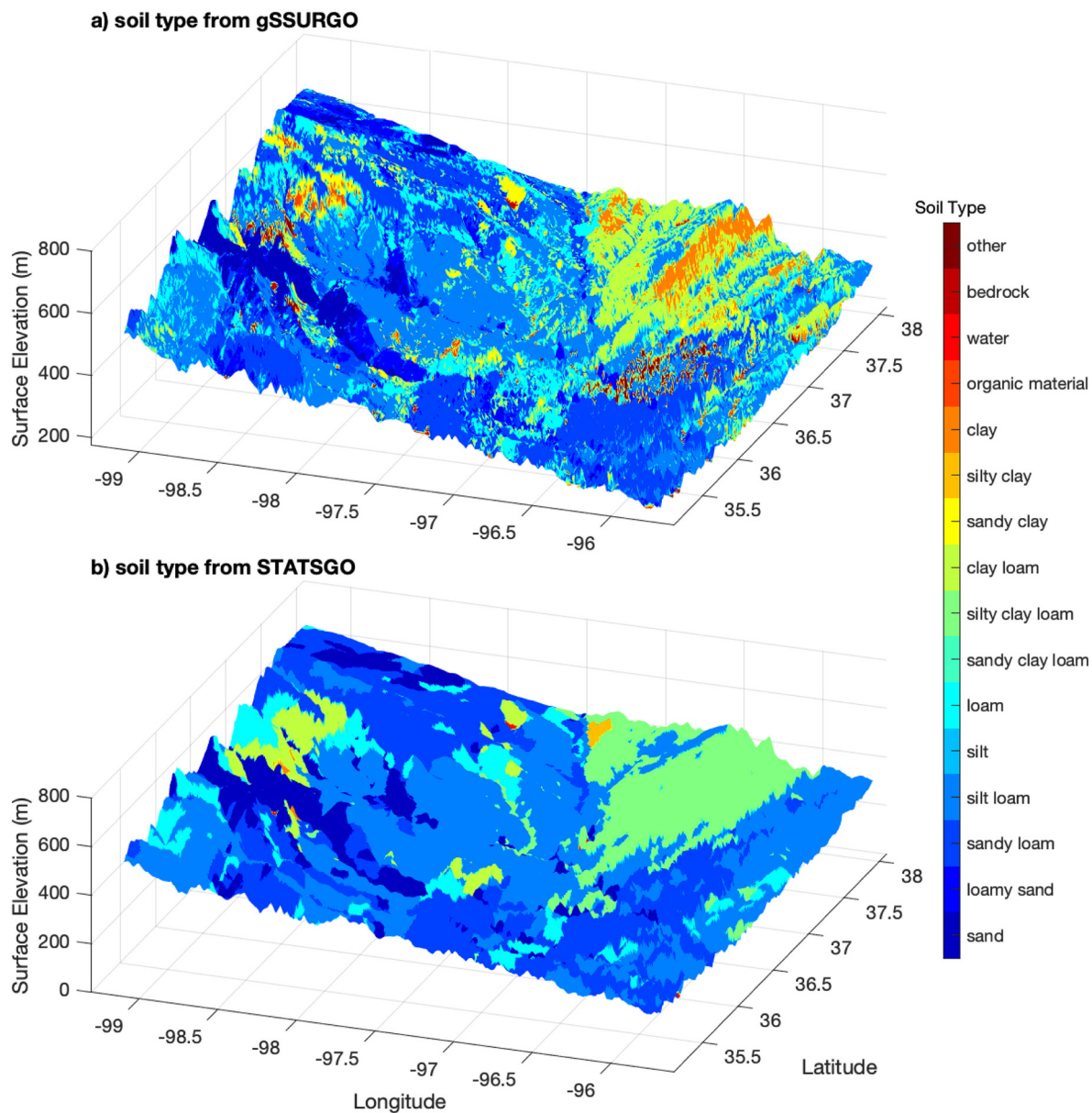


**Figure 2.** Soil type data sets obtained by interpolating from (a) the Gridded Soil Survey Geographic (gSSURGO) and (b) the default State Soil Geographic (STATSGO) data sets.

incoming shortwave and longwave radiation, specific humidity, air temperature, surface pressure, zonal ( $u$ ) and meridional ( $v$ ) components of near surface wind, and precipitation rate. Digital Elevation Map (DEM) data are obtained from the Hydrological data and maps based on the National Hydrography Data set Plus Version 2 (NHDPlusV2, McKay et al., 2012). NHDPlusV2 integrates the vector stream network, hydrologic unit boundaries with the National Elevation Dataset (NED) gridded land surface. It also provides stream order and a group of attributes that facilitate rapid stream network traversal and query. The DEM data set is processed with the Arcgis toolbox provided by the WRF-Hydro community to obtain the land surface characteristics that are related to surface/subsurface routing.

The default soil texture data used in the study are from the State Soil Geographic (STATSGO) database (see Figure 2; Miller & White, 1998). It was created by generalizing published and unpublished soil-survey maps, country and state general maps, state major land resource area maps, and Landsat imagery. Another soil texture data set, the Gridded Soil Survey Geographic (gSSURGO) Database available at 30 m grid spacing,

**Table 1***Model Specifications for the Default Noah-MP Simulation (A1)*

Physical processes	Options
Dynamic vegetation	4 (use Table LAI; maximum vegetation fraction)
Canopy stomatal resistance	1 (Ball-Berry)
Soil moisture factor for stomatal resistance	1 (Noah)
Runoff and groundwater	3 (original surface and subsurface free drainage)
Surface layer drag coefficient	1 (M-O)
Supercooled liquid water	1 (no iteration)
Frozen soil permeability	1 (linear effects, more permeable)
Radiation transfer	3 (two stream applied to vegetation fraction)
Ground snow surface albedo	2 (CLASS)
Partitioning precipitation into rainfall and snowfall	1 (Jordan, 1991)
Lower boundary condition of soil temperature	2 (TBOT at ZBOT read from a file)
Snow-soil temperature time scheme	3 (same as 1, but FSNO for TS calculation)
Surface resistance to evaporation/sublimation	4 (Sakaguchi & Zeng, 2009 for non-snow, rsurf = rsurf_snow for snow)

Abbreviation: LAI, leaf-area index.

is also included in this study. The gSSURGO Database is derived from the official Soil Survey Geographic (SSURGO) Database and it has the most detailed level of soil geographic data that is developed by the National Cooperative Soil Survey (NCSS) in accordance with NCSS mapping standards. We also compare it with observations collected at multiple sites within the US DOE's ARM Climate Research Facility SGP observatory.

The default soil hydraulic parameters in the model are obtained by mapping to the specified soil types following a lookup table originally developed by Cosby et al. (1984). However, the values have not been updated for 25 years and some soil hydraulic parameters show sizable biases when compared with recent estimations (C. Zhang, Xie, et al., 2018; Y. Zhang, Schaap, & Zha, 2018). Kishn   et al. (2017) proposed a new soil parameter table based on measured soil properties from 6,749 soil samples located within and around Texas. The authors reported that 95% of the soil parameters are significantly different from the measured values. Sensitivity tests are performed to estimate the uncertainty associated with using different soil lookup tables in this study. For the values of the updated soil hydraulic properties, readers are referred to Table 6 in Kishn   et al. (2017).

The WRF-Hydro model is run with the default NLDAS-2 precipitation as well as the Stage-IV precipitation (Du, 2011). The 4-km Stage-IV precipitation were scaled up to a resolution of 0.125° to match NLDAS-2 while preserving grid-mean precipitation and then interpolated to the grid resolution as input forcing to drive the model. Here we assume that the Stage-IV precipitation is more accurate given it is able to capture the convective precipitation during the warm season. In fact, a comparison to gauge precipitation at the SGP central facility reveals that the Stage-IV precipitation reduces the mean absolute bias by around 4.5% compared to the NLDAS-2.

#### 2.4. Experiment Design

To elucidate the effect of initial and boundary conditions, the lateral flow process, and resolution dependence on soil moisture and surface fluxes, we designed several experiments in this study. Each experiment is based upon the previous experiment to isolate the role played by different components for how they affect the soil moisture and surface fluxes. The baseline default Noah-MP (A1) simulation is run with nominal 1 km grid spacing with 392 grid cells in the zonal and meridional directions. It uses the default tabular values of LAI and maximum vegetation fraction as a function of land use/land cover, Ball-Berry for canopy stomatal resistance, free drainage for runoff option, and Monin-Obukohov for surface layer drag coefficient (see Table 1 for more details). Starting from the default experiment (A1), we replaced the soil with

**Table 2***Description of Simulation Plan and their Objectives*

	Description	Objective
A1	Default NLDAS-2 input	-
A2	Same as A1, with new gSSURGO soil data set	The sensitivity of soil data set
A3	Same as A2, with new soil parameter table.	The sensitivity of new soil parameter table
A4	Same as A3, with climatological mean GVF and LAI from MODIS	The effect of dynamic vegetation
A5	Same as A3, with actual GVF and LAI from MODIS	
A6/B1	Same as A5, with Stage-IV precipitation as input	The effect of precipitation input forcing
A7	Same as A6, with surface lateral flow	The effect of lateral flow
A8	Same as A6, with subsurface lateral flow	
A9	Same as A6, with lateral and subsurface lateral flow	
B2	Same as A9, LSM at 1 km, routing at 100 m	Check the effect of LSM resolution and routing resolution
B3	Same as A9, LSM at 1 km, routing at 250 m	
B4	Same as A9, LSM at 1 km, routing at 500 m	
B5	Same as A9, LSM at 1 km, routing at 1,000 m	
C1	Same as A6, LSM at 4 km, no routing	
C2	Same as A9, LSM at 4 km, routing at 100 m	
C3	Same as A9, LSM at 4 km, routing at 250 m	
C4	Same as A9, LSM at 4 km, routing at 500 m	
C5	Same as A9, LSM at 4 km, routing at 1,000 m	
D1	Same as A6, LSM at 10 km, no routing	
D2	Same as A9, LSM at 10 km, routing at 250 m	
D3	Same as A9, LSM at 10 km, routing at 500 m	
D4	Same as A9, LSM at 10 km, routing at 1,000 m	

*Note.* Format tables using the Word Table.

Abbreviations: gSSURGO, Gridded Soil Survey Geographic; GVF, Greenness Vegetation Fraction; LAI, leaf-area index; LSM, land surface model; NLDAS-2, National Land Data Assimilation System Phase 2.

the gSSURGO soil type in A2. By comparing A1 and A2, we could examine the effect of soil type (e.g., see Table 2). Similarly, the soil parameter lookup table in A2 is updated with the new table developed by Kishné et al. (2017) in A3. By comparing A2 and A3, one may examine the effect of different soil lookup tables (Table 2).

The default vegetation option in the Noah-MP model uses the maximum Greenness Vegetation Fraction (GVF) derived from the climatological MODIS mean from 2001 to 2010 and LAI interpolated from an empirical lookup table based on land use and land cover type (DVEG = 4). There is also an option available in Noah-MP that uses the actual GVF and LAI (DVEG = 7). The MODIS real-time GVF and LAI observations (MYD15A2H, Myneni et al., 2015) provides the opportunity to feed the model with actual vegetation conditions. The MYD15A2H products closest to the middle of each month are extracted for the whole simulation period. For each year, there are 12 sets of GVF and LAI to represent the monthly value. First, these multi-year monthly GVF and LAI are averaged to obtain a climatological mean for each month. They are then ingested into A4 to represent the climatological mean vegetation conditions. A5 represents an experiment with near real-time MODIS GVF and LAI. Ideally, A5 is more realistic in terms of vegetation representation than A3 and A4. By comparing A3 and A4, one could estimate the effect of using maximum GVF and table-based land cover-dependent LAI versus the climatological GVF and LAI. By comparing A4 and A5, we could examine the effect of climatological versus the near real-time GVF and LAI.

On the basis of A5, A6 examines the effect of using Stage-IV precipitation versus the NLDAS-2 default precipitation. A7 and A8 switch on the surface and subsurface flow, respectively, while A9 turns on both

surface and subsurface routing. The surface lateral flow uses the steepest gradient “D8” method (Table 2). It should be noted that for experiments A1–A6, run without lateral flow components, we are actually evaluating the performance of the Noah-MP model. It is important to note that the results shown later are prone to the underlying assumptions and uncertainties associated with the Noah-MP. The combinations B1–B5, C1–C5, and D1–D4 examine the effect of routing resolution with LSM grid spacings of 1, 4, and 10 km, respectively. Note that at each LSM resolution, we make sure that channel density remains the same at the preprocessing stage by ensuring that the area of routing grid cells to define stream is the same across different routing resolutions.

### 3. Evaluation of WRF-Hydro

#### 3.1. Evaluating the Impact of Input Forcings

This section aims to evaluate the effect of different soil type, soil parameter table, vegetation, and precipitation. We emphasize that this study should be considered as a sensitivity study, since we did not calibrate the WRF-Hydro and our focus is more on evaluating the effect of model inputs and the routing processes.

##### 3.1.1. Soil Texture and Soil Parameters

The default STATSGO and gSSURGO soil data sets, when interpolated to the model domain at 1 km grid spacing, are shown in Figure 2. The overall spatial pattern of the two data sets agrees reasonably well. The dominant soil types are silt and silt loam, distributed mainly in the southern and central domain, whereas silty clay loam and clay loam is predominant over the northeastern part. However, there are also clear differences between these two data sets. The gSSURGO shows much more detail than the STATSGO. For example, some of the stream networks are clearly seen in the gSSURGO data set but are missing in the STATSGO. Inconsistencies exist between these two data sets, as about 45% of the grid cells are identified differently. Compared to the STATSGO, the gSSURGO presents a larger percentage of sand, sandy loam, silt loam, and silty clay loam, and less percentages of loamy sand, loam, clay loam, silty clay, and clay (Figure S1). The conversion from sand in STATSGO to other soil types in gSSURGO consistently leads to an increase in LH, resulting in an overall increase of  $+0.96 \text{ W m}^{-2}$ , whereas the conversion from silt loam in STATSGO to other soil types in gSSURGO leads to a decrease of  $-0.65 \text{ W m}^{-2}$  in LH. More details on the impact of soil type differences can be seen in Figure S2. Changes in SH is of the same magnitude but with opposite sign. On average, changing from STATSGO to gSSURGO leads to about  $0.18 \text{ W m}^{-2}$  increase in SH and decrease in LH.

We have also compared the soil type data collected at the STAMP sites; the gSSURGO is not superior or more accurate than the STATSGO when compared to the in situ measurements. Out of the 16 STAMP stations, both data sets have six sites that are consistent with the observed soil type. We note that this is not an exact fair comparison, since gSSURGO and STATSGO both are at 1 km resolution and represent the dominant soil type within nearest grid cell to the observation, whereas STAMP represents a point-collected soil sample. Nevertheless, the resulting difference in soil hydraulic parameters are quite large due to the use of different soil type data sets. The difference in soil property parameters due to the use of different soil parameter tables is shown in Figure 3. These changes in soil hydraulic parameters induce changes in soil moisture and surface energy heat fluxes. Sensitivity tests suggest that maximum soil moisture content (MAXSMC) and soil conductivity (SATDK) show the strongest control on the energy fluxes, whereas MAXSMC and wilting point soil moisture (WLTSMC) have the strongest impact for soil moisture (Figures S3–S5). The results here are consistent with Cuntz et al. (2016), in which the authors also identified that MAXSMC and SATDK are the most sensitive parameters that control the land-atmosphere fluxes exchange and surface runoff.

When the new soil parameter table is used, the simulated soil moisture decreases for loamy sand, sandy loam, and clay loam, but increases for other soil types, especially for sand and clay (Figure 4a). For the energy fluxes, latent heat fluxes increase for sand and clay, but decrease for other soil types, of which sandy loam and silty clay loam show the strongest decrease (Figure 4b). The opposite is true for sensible heat flux, except for loamy sand, of which both latent heat flux and sensible heat flux decrease (Figure 4c).

Another interesting thing is that even though soil moisture increases for silt loam, loam, silty clay loam, silty clay, and organic material, LH (SH) decreases (increases) for these soil types. This is likely because the

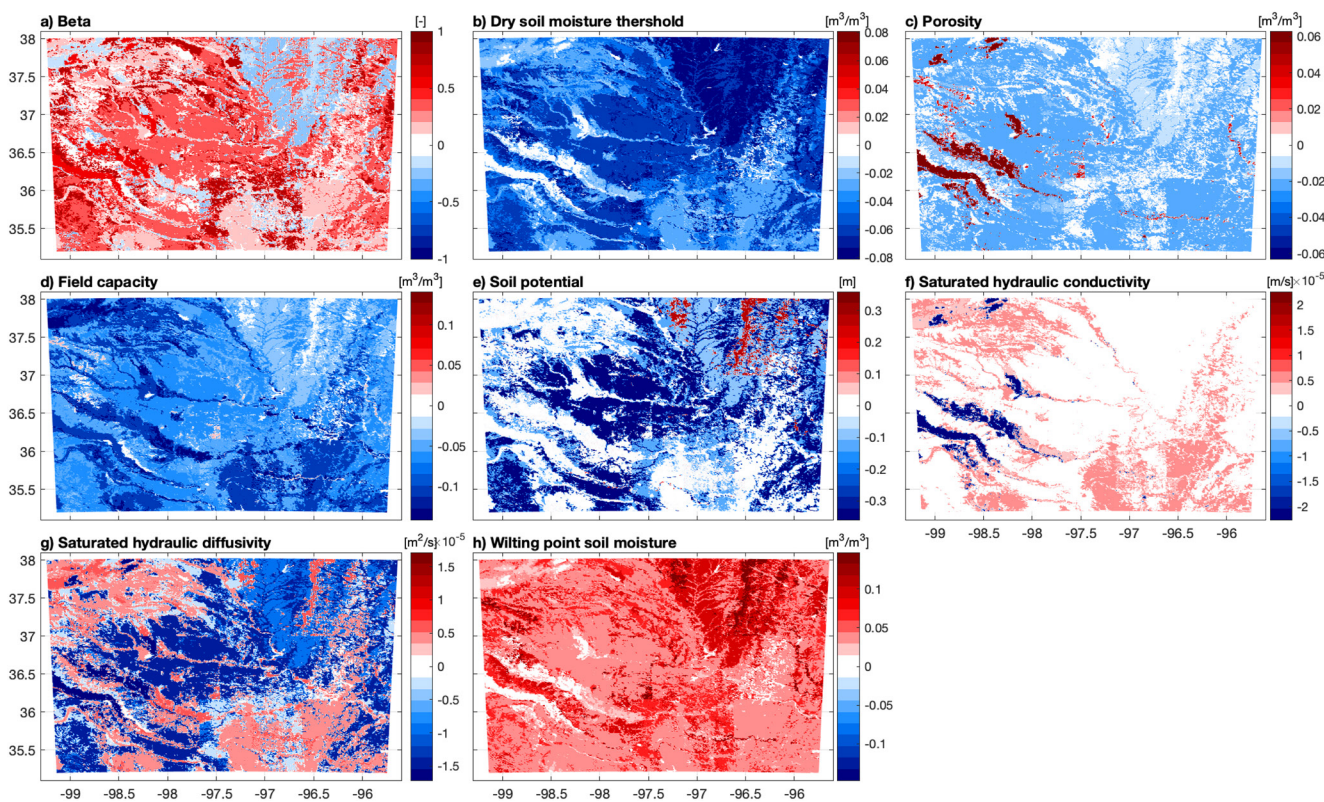


**Figure 3.** Differences in soil hydraulic properties induced by using the new soil parameter table from Kishné et al. (2017), as opposed to the default soil parameter table.

wilting point of these soil types are increased and as a result it is easier for soil moisture to decline to the wilting point and soil evaporation more easily ceases being a limit on latent heat flux.

Comparing sand with loam, the sign of changes in soil properties are all the same, except for SATDK (Figures S6 and S7). For SATDK, the positive change of loam and negative change of sand resulted in decreased LH for loam, but increased LH in sand. This is likely because increased SATDK allows water to more efficiently exchange water within the soil column and drain it out the bottom, instead of preserving water within the soil column. Similarly, comparing sand with silt loam, the only difference is that porosity of silt loam is decreased whereas that of sand is increased when the new soil parameter table is used (Figures S6 and S8), resulting in increased LH in sand, but decreased LH for silt loam. This suggests that a larger porosity is more likely to introduce higher LH.

### 3.1.2. Comparison to Observations

Since different inputs and boundary forcings have been considered in this study; here we try to compare them within the same context. Figure 5 shows the average monthly time series of LH at the EBBR and ECOR observation stations with the model values extracted at the nearest grid cells. The model captures the overall trend of the monthly time series, although it is suggested that utilizing more realistic data does not ensure better results. This is likely associated with the model deficiencies, since the default parameters are optimized for global scale simulations (Niu et al., 2011; Z.-L. Yang et al., 2011). In general, the model underestimates latent heat flux across all model experiments, which has been a known issue for land surface models over the Great Plains (e.g., Lin et al., 2017; Ma et al., 2018; Morcrette et al., 2018; Van Weverberg et al., 2018; C. Zhang, Xie, et al., 2018; Y. Zhang, Schaap, & Zha, 2018).

The detail statistics of comparison between model simulations and observations, in terms of model mean bias, root mean square error and Pearson's correlation coefficient ( $R$ ) are shown in Tables S1 and S2 for LH and soil moisture in the Supplementary information. In general, when compared to observations the

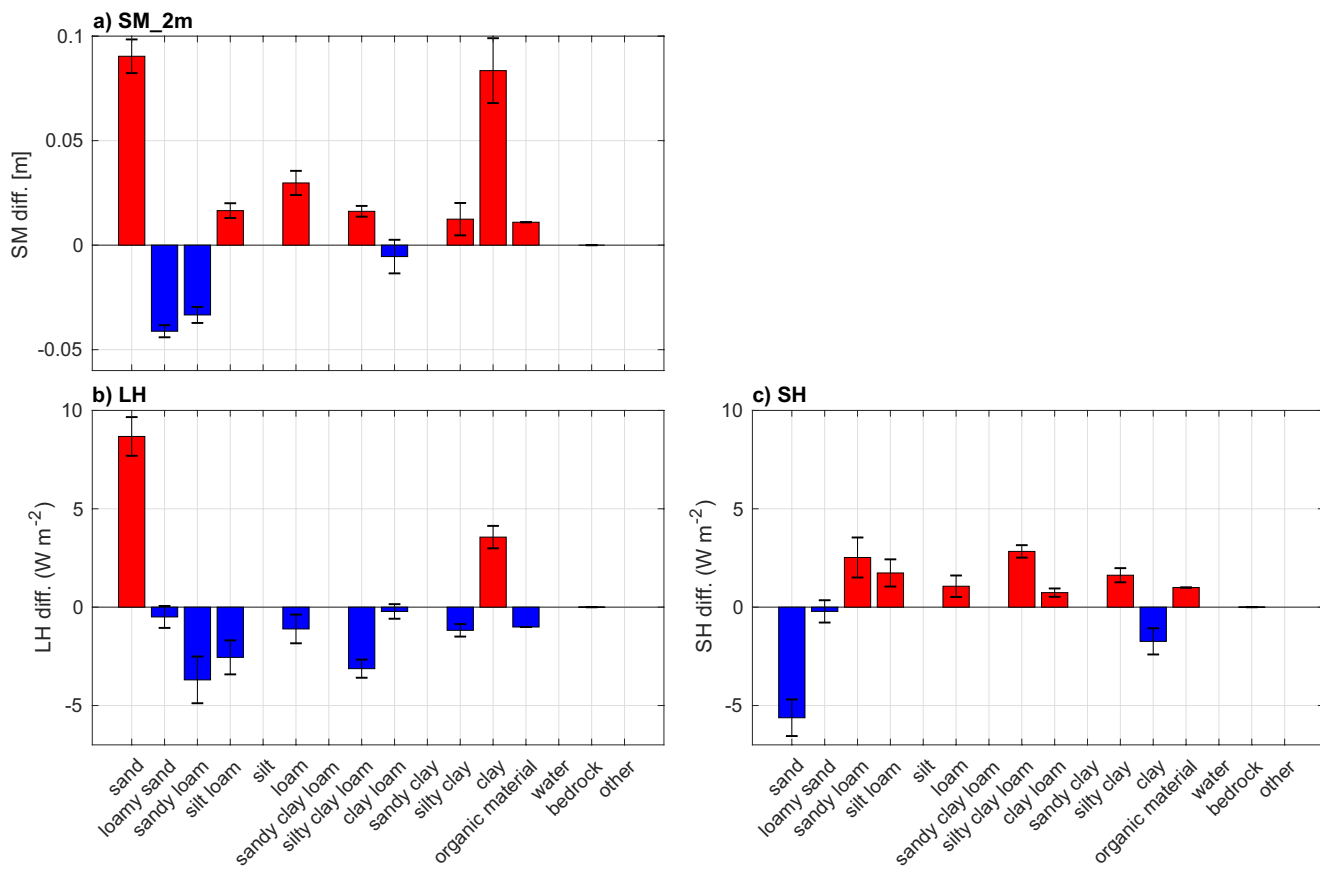


**Figure 4.** Average difference for each soil type by using the new soil parameter table as opposed to the default soil parameter table for (a) column integrated soil moisture (top 2 m) (b) latent heat flux (LH), and (c) sensible heat flux (SH). The error bar indicates one standard deviation.

differences in error statistics between the suite of simulations are quite small. One possible reason is that these comparisons are performed only at the ARM sites where observation are available, where the differences are relatively small. There are other locations in the domain where the differences are significantly larger (shown later). More specifically, the gSSURGO data show a nearly negligible effect on the monthly averaged latent heat flux (Figure 5a); the use of the new soil parameter table slightly reduces the latent heat flux and leads to a larger underestimation (Figure 5b); the use of the maximum GVF, although is seemingly unrealistic, in fact produces the best result as compared to the experiments with realistic MODIS GVF (Figure 5c). Additionally, the use of time-varying GVF and LAI does not yield significantly different LH than using the climatological GVF/LAI (Figure 5c). Although Stage-IV precipitation is deemed as more realistic, it leads to larger underestimation of latent heat flux (Figure 5d). The consideration of lateral flow partly alleviates the underestimation of LH and slightly improves the performance of LH (Figure 5e). The use of different routing resolution induces some seasonal differences. Routing resolution only starts to show an impact below 500 m resolution over the summer months, and above 500 m they are almost identical when averaged over the ARM sites (Figure 5f).

Figure 5 clearly indicates that the differences induced by different model configurations show clear distinctions in summer than in other seasons. Figure 6 shows the comparison of soil moisture to observations collected from the STAMP sites in June, July, and August (JJA) 2016. Only 2016 is shown because of data availability. Compared to the STAMP sites, all configurations clearly overestimate soil moisture. Given the underestimation in LH in Figure 5, it suggests that the Noah-MP needs to evapotranspire more through either direct soil evaporation or transpiration to simultaneously reduce the biases in soil moisture and latent heat flux. Specifically, the use of new soil type data and Stage-IV precipitation forcing decrease the bias in soil moisture while the new soil table and MODIS dynamic vegetation slightly increases the soil moisture bias. The routing scheme mainly increases soil moisture and, therefore, increases the soil moisture bias.

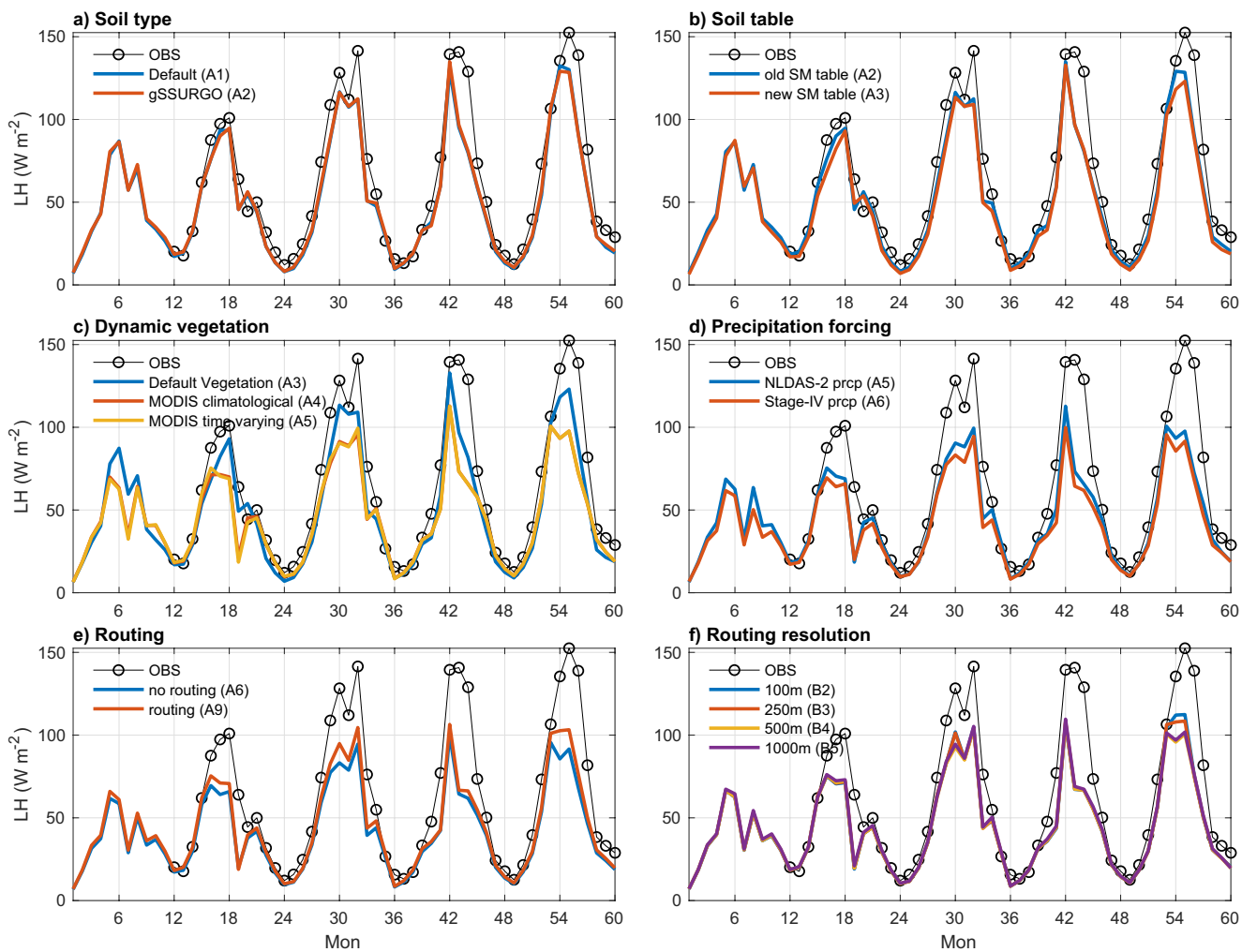


**Figure 5.** Comparison between monthly mean latent heat flux at the energy balance Bowen ratio and eddy correlation stations and Weather Research and Forecasting-Hydro simulation for 2011–2015. Each panel was designed to isolate the effect of (a) soil type data set of State Soil Geographic (A1) versus Gridded Soil Survey Geographic (A2), (b) soil parameter table from Cosby et al. (1984) (A2) versus from Kishné et al. (2017) (A3), (c) default dynamic vegetation (A3) versus MODIS climatology (A4) versus MODIS real time (A5), (d) precipitation from NLDAS-2 (A5) versus Stage-IV (A6), (e) without lateral flow (A6) versus with surface and subsurface lateral flow (A9), and (f) different routing resolution for lateral flow.

### 3.2. Effects of Routing

Figure 7 shows the spatial pattern of soil moisture differences induced by using different routing options, including no routing (A6), surface routing only (A7), subsurface routing only (A8), and both surface and subsurface routing (A9). The difference fields thus can isolate the effect of surface versus subsurface lateral flow and their interaction as simulated by the WRF-Hydro model. Note these experiments are simulated at 1-km LSM and 250-m routing grid spacing. Including surface lateral flow consistently increases soil moisture across the soil column, but mostly only over the lower-elevation convergence regions. For steeper terrain in the southwest of the domain, surface flow does not show noticeable impact on soil moisture (Figures 7a, 7d, 7g, and 7j). This is because surface lateral flow very efficiently redistributes water from the steep slopes toward lower elevations. The subsurface lateral flow, besides increasing soil moisture over the flat terrain at lower elevations, also leads to variable changes in the soil column over the peaks in the Southwest (Figures 7b, 7e, 7h, and 7k). Soil moisture is increased in the top layers and decreased in the bottom layers, which is associated with the re-infiltration processes. Over steeper terrains, lateral flow from the soil column will increase soil moisture content at shallower layers at the next downstream soil column, while decreasing deep layer soil moisture in the current soil column. When both surface and subsurface routing

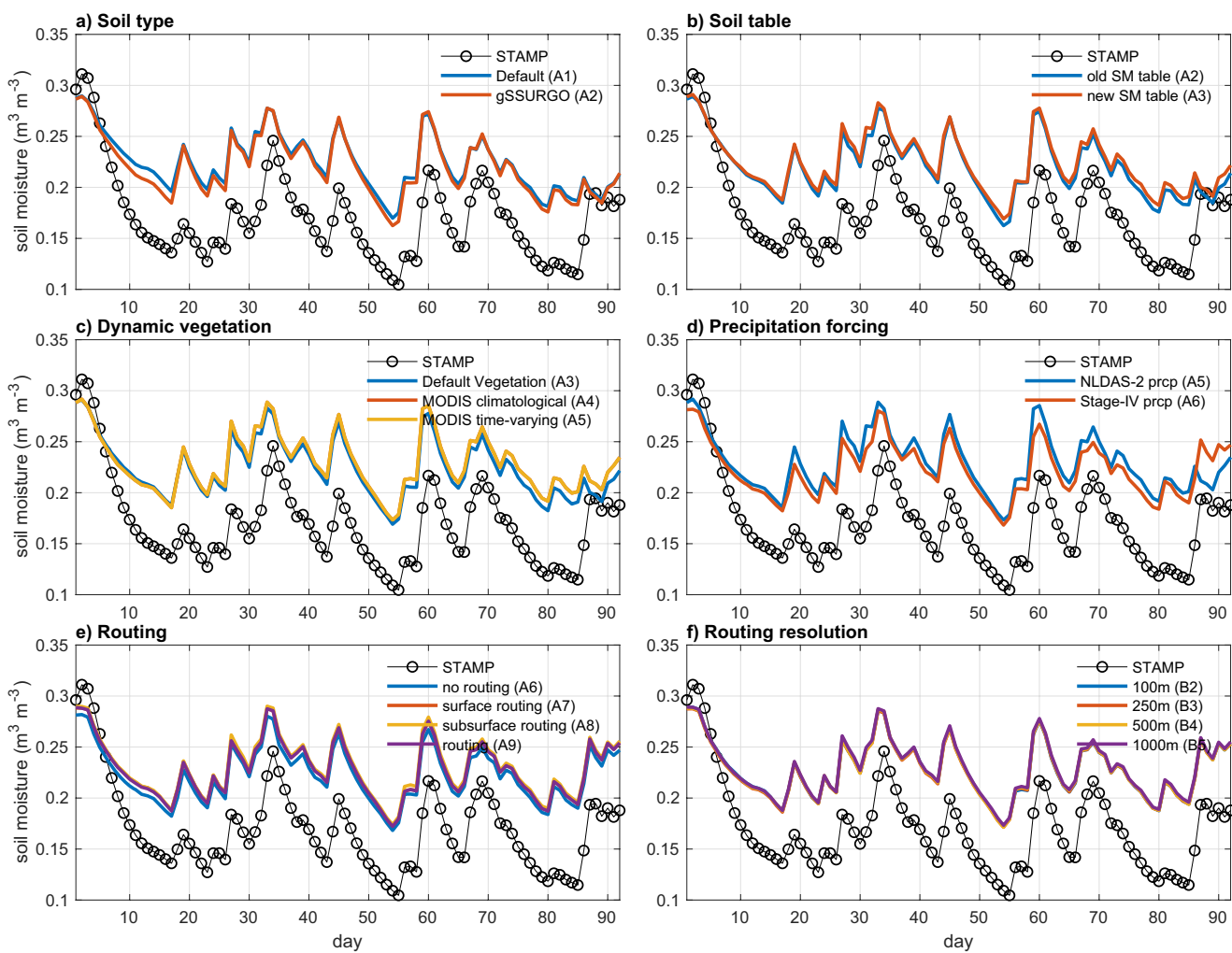


**Figure 6.** Comparison of soil moisture at 5 cm depth between Soil Temperature and Moisture Profiles (STAMP) stations and Weather Research and Forecasting-Hydro simulations for June-July-August in 2016. Each panel is similar to Figure 5 but for soil moisture.

are turned on, almost the entire domain experiences an increase in the soil moisture content, with the exception of the deeper layer over the steepest terrain in the southwest (see Figures 7c, 7f, 7i, and 7l). The reduced soil moisture over the steep terrain is mainly associated with subsurface lateral flow. The response of LH and SH to different routing choice is shown in Figure 8. In general, the response of LH shows a very similar pattern as the soil moisture, while SH shows the opposite.

It is interesting to note that the difference between both routing (A9) and subsurface routing only (A8), which is also often treated as an indication of surface flow effect, has a different pattern than the difference between surface routing (A7) and no routing (A6) (see difference in first and third column in Figure 7). In fact, the difference between simulations with (A7) and without (A6) surface lateral flow shows the isolated effect of surface lateral flow only, whereas difference between simulation with both lateral surface and subsurface (A9) and with subsurface routing only (A8) includes surface effects as well as the interaction between surface and subsurface lateral flow (see Equation 1 below). The interaction between surface and subsurface routing turns out to reduce the soil moisture content (Figure 9), meaning that both surface and subsurface lateral flows are efficiently removing moisture from the soil columns to deep drainage or channel networks.

$$\text{Interaction} = \text{both routing} - \text{surface routing} - \text{subsurface routing} + \text{no routing} \quad (1)$$

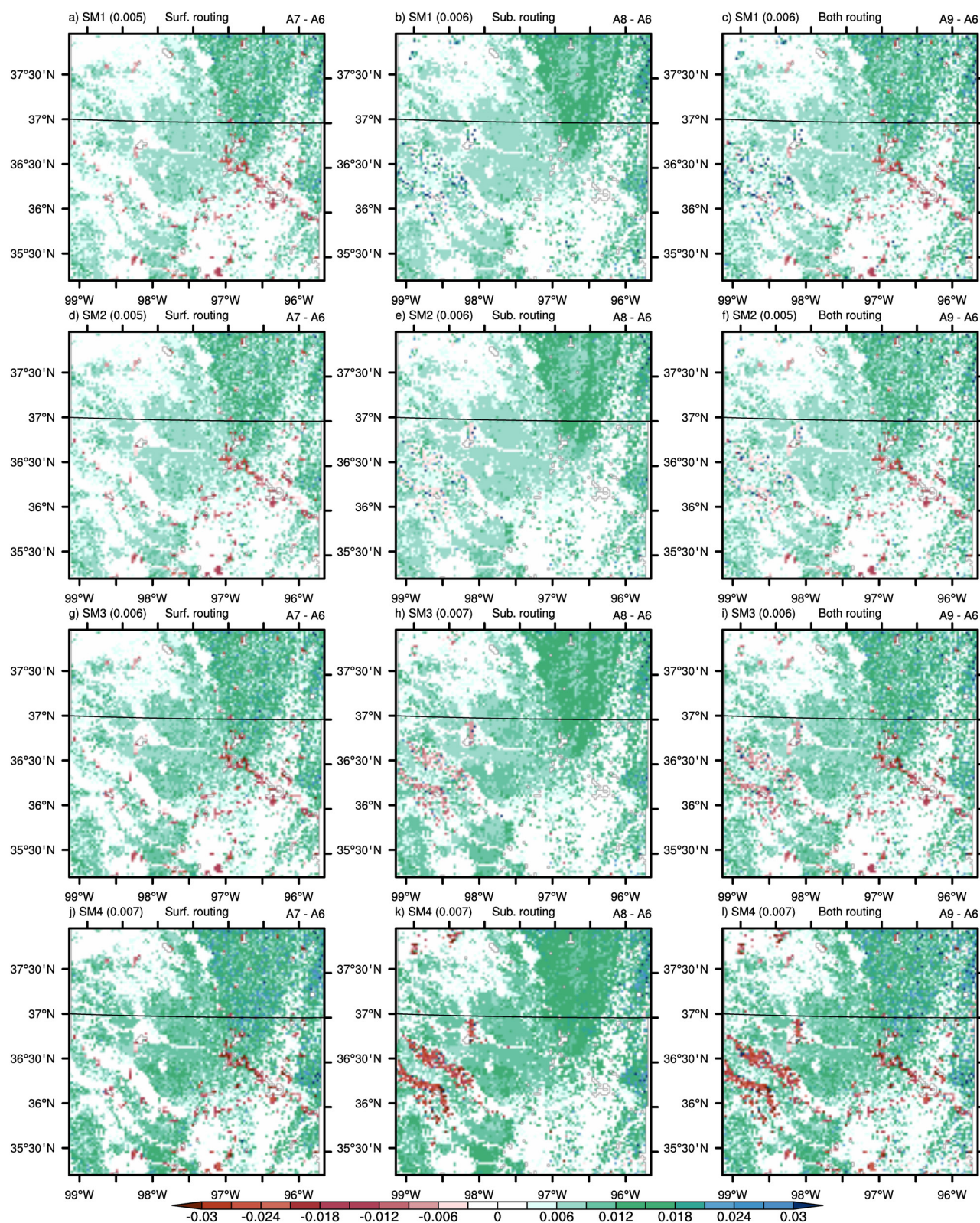


**Figure 7.** Annual averaged soil moisture difference induced by different routing choices. (a, d, g, and j) Difference in soil moisture between surface routing (A7) and no routing (A6) in different soil layers. (b, e, h, and k) Difference between subsurface routing (A8) and no routing (A6). (c, f, i, and l) Difference between both surface and subsurface routing only (A9) and no routing (A6). Numbers in the parenthesis are the domain average (units:  $\text{m}^3 \text{ m}^{-3}$ ). The black line at  $37^\circ\text{N}$  is the border between Oklahoma and Kansas.

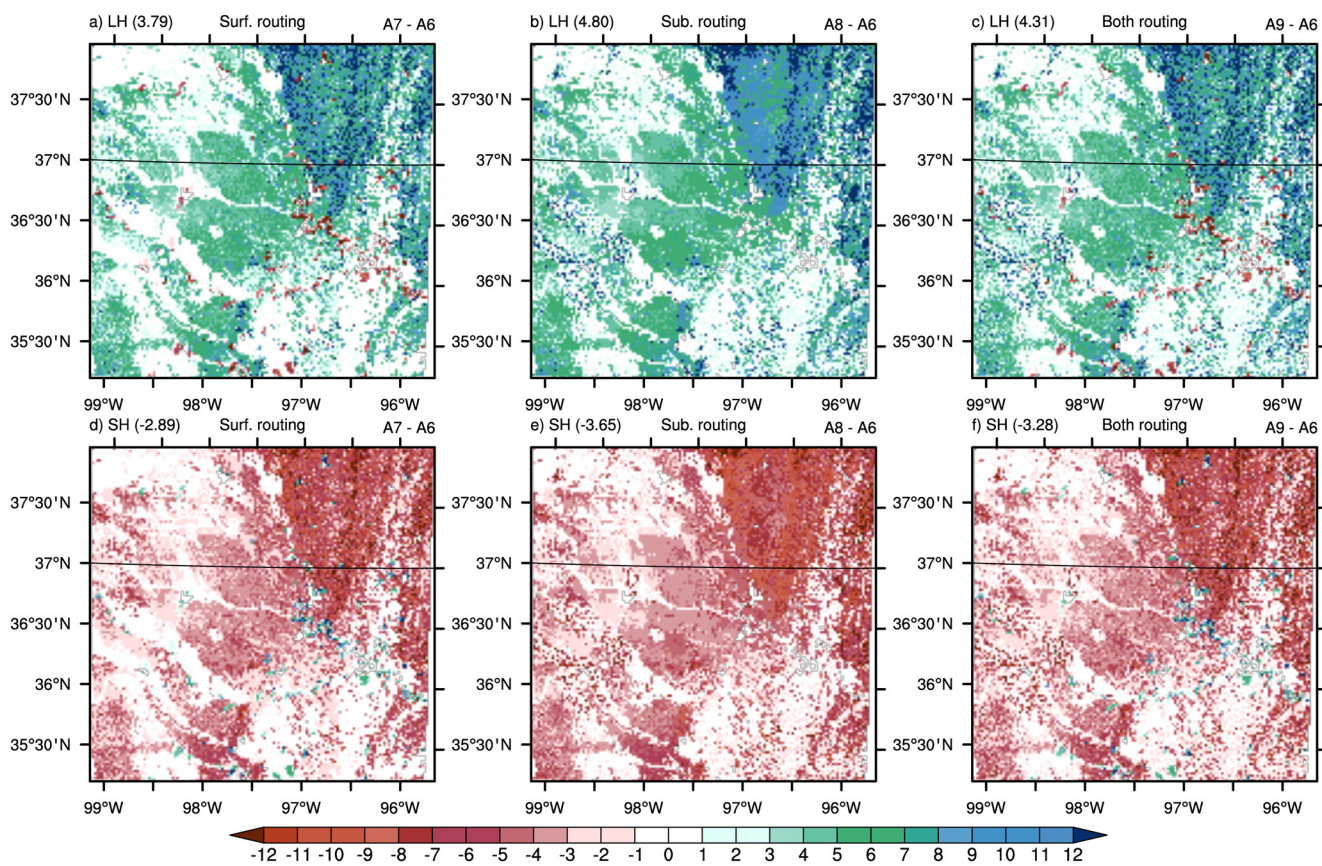


**Figure 8.** Similar as Figure 7, but for sensible heat flux (SH) and latent heat flux (LH), units:  $\text{W m}^{-2}$ . Numbers in the parenthesis are the domain average (units:  $\text{W m}^{-2}$ ).

### 3.3. Effects of Land Surface and Routing Resolution

This section aims to address the question of how land surface variables react to the resolutions of LSM and routing schemes. WRF-Hydro is designed such that the resolutions of LSM and routing schemes can be different by using the disaggregation-aggregation methodology. Before the routing starts, the surface variables from the LSM are disaggregated to the routing grid cells, and then aggregated to the LSM grid cells when then routing scheme finishes. To test the impact of resolution, land surface grid spacing is chosen at 1, 4, and 10 km, while routing grid spacing is chosen at 100, 250, 500, and 1,000 m. Experiments are performed with each pair of LSM and routing resolution listed above, with the exception of LSM at 10 km and routing grid spacing at 100 m.

Figure 10 shows the difference in soil moisture due to the change in routing grid spacing when LSM grid spacing is at 1 km. Overall, there are consistently higher soil moisture contents over the steep terrain when higher routing resolution is used. The difference fields are consistent for all four soil layers with a similar magnitude. When a coarser routing resolution is used for routing, soil moisture is smaller than in simulations with higher routing resolution, indicating that routing resolution is important in regulating the simulated soil moisture content, with higher routing resolution leading to larger soil moisture content, especially over steeper terrains.

A similar transition in the difference fields is also found when the LSM grid spacing is coarser at 4 and 10 km, except that the difference field is almost negligible between routing at 100 and 250 m when LSM grid spacing is 4 km, and between 250 and 500 m when LSM grid spacing is 10 km (see Figures 11 and 12), meaning that routing does not add extra value at 100 m (250 m) grid spacing for 4 km (10 km) LSM grid spacing, although the computation cost for routing is roughly about  $\sim 10$  times that of routing at 250 m (500 m). Since the difference only shows for steeper terrain, it suggests that the slope of the terrain is an

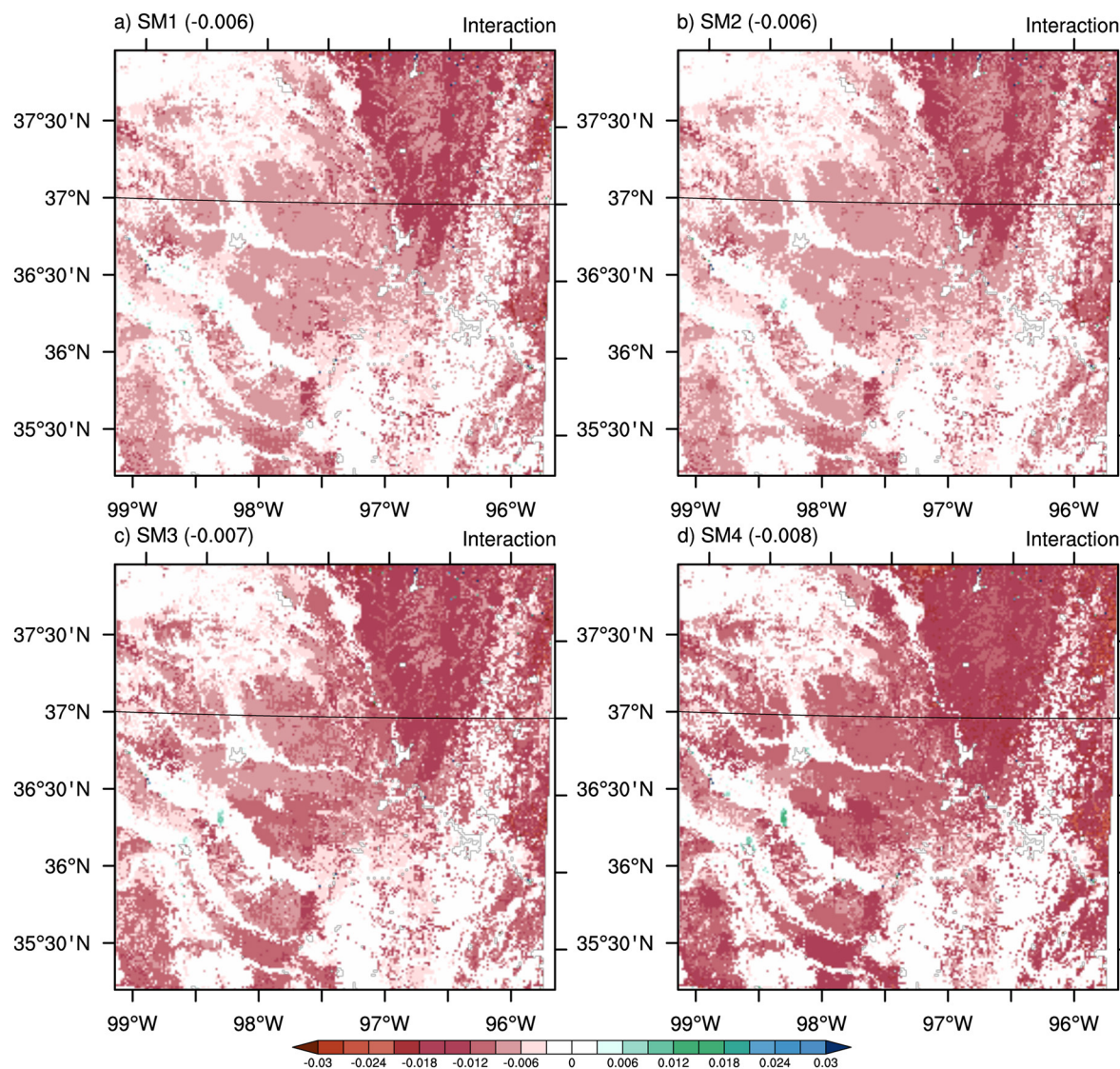


**Figure 9.** Effect of interaction between surface and subsurface routing on soil moisture at different soil layers, as represented by Equation 1. Numbers in the parenthesis are the domain average (units:  $\text{m}^3 \text{ m}^{-3}$ ).

important factor controlling the changes in soil moisture induced by routing resolution. Figure 13 presents the relationship between routing induced soil moisture difference and the slopes at different LSM resolutions. Some general conclusions are synthesized as follows:

1. At the same LSM resolution, soil moisture generally decreases with a coarser routing resolution especially over the steeper regions. Or in other words, the difference between the finest and coarsest routing resolutions always displays the largest difference.
2. Soil moisture difference induced by routing resolution over the steep terrain is more obvious in the shallow soil layers, and this discrepancy is more obvious when LSM resolution is higher.
3. Soil moisture is less sensitive to the chosen routing resolution when LSM resolution is coarser, that is, when LSM resolution is coarser, the difference in soil moisture due to different routing resolution gradually fades out.

The calculation of water balance following Thornthwaite (1948) and Mather (1978) helps to illustrate the reason why differences are shown between high- and low-resolution routing. The water balance equation is as follows:

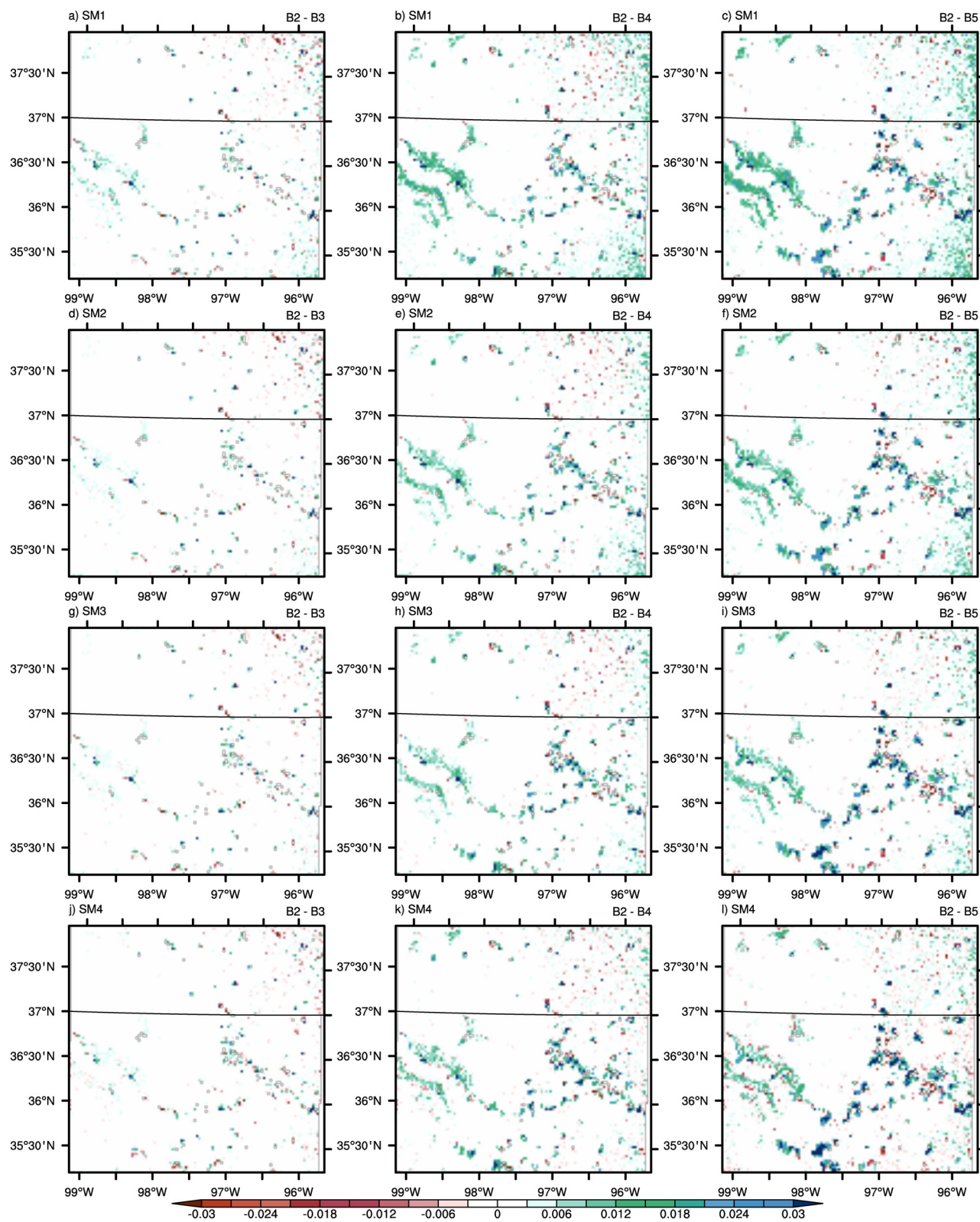


**Figure 10.** At 1 km land surface model grid spacing, differences in soil moisture between different routing resolution at different soil layers. (a, d, g, and j) Soil moisture difference at different soil layers induced by routing at 100 m (B2) and routing at 250 m (B3). (b, e, h, and k) are similar as (a, d, g, and j) but for difference between routing at 100 m (B2) and 500 m (B4). (c, f, i, and l) are similar as (a, d, g, and j) but for difference between routing at 100 m (B2) and 1,000 m (B5).

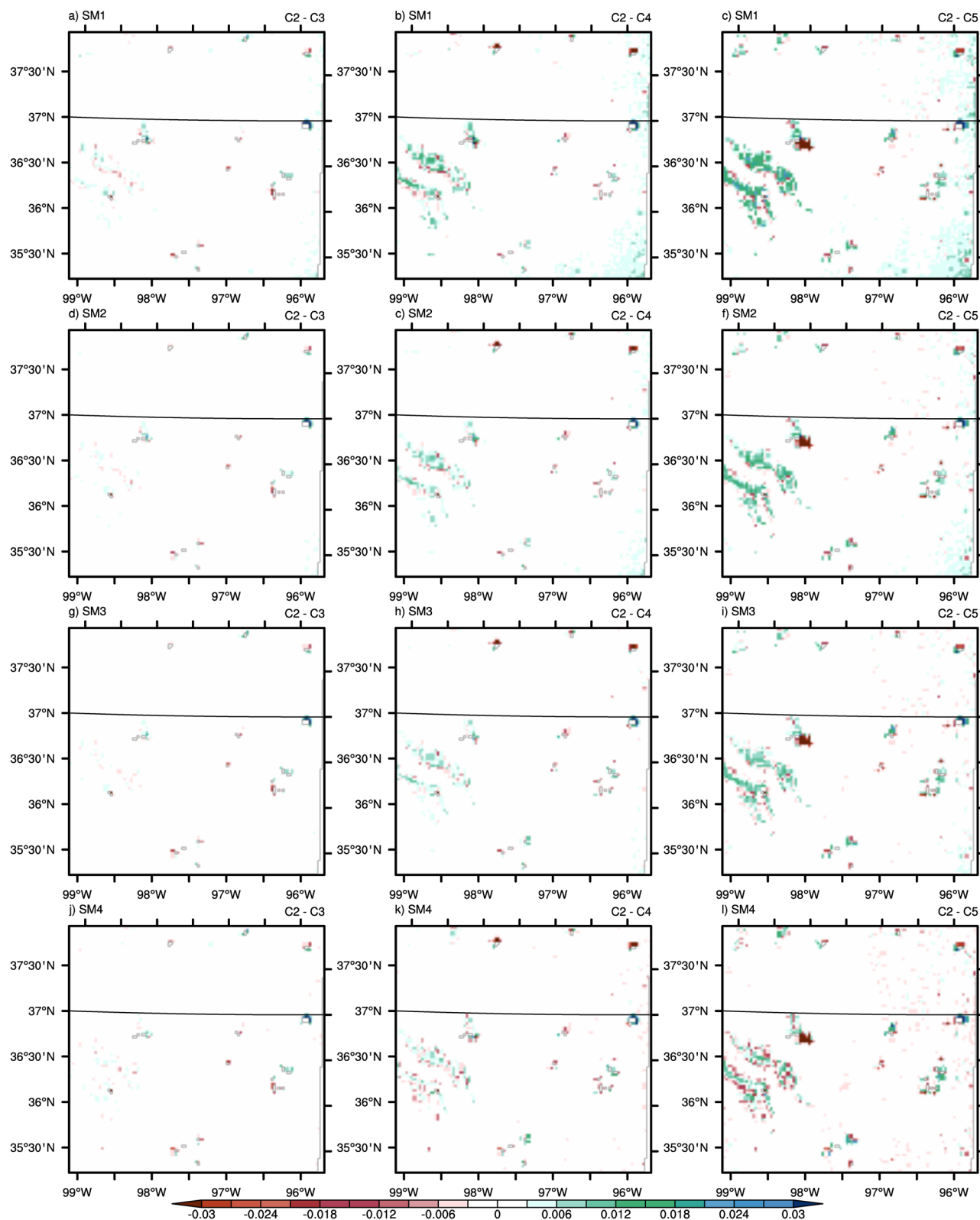


**Figure 11.** Similar as Figure 10, but for land surface model resolution at 4 km.

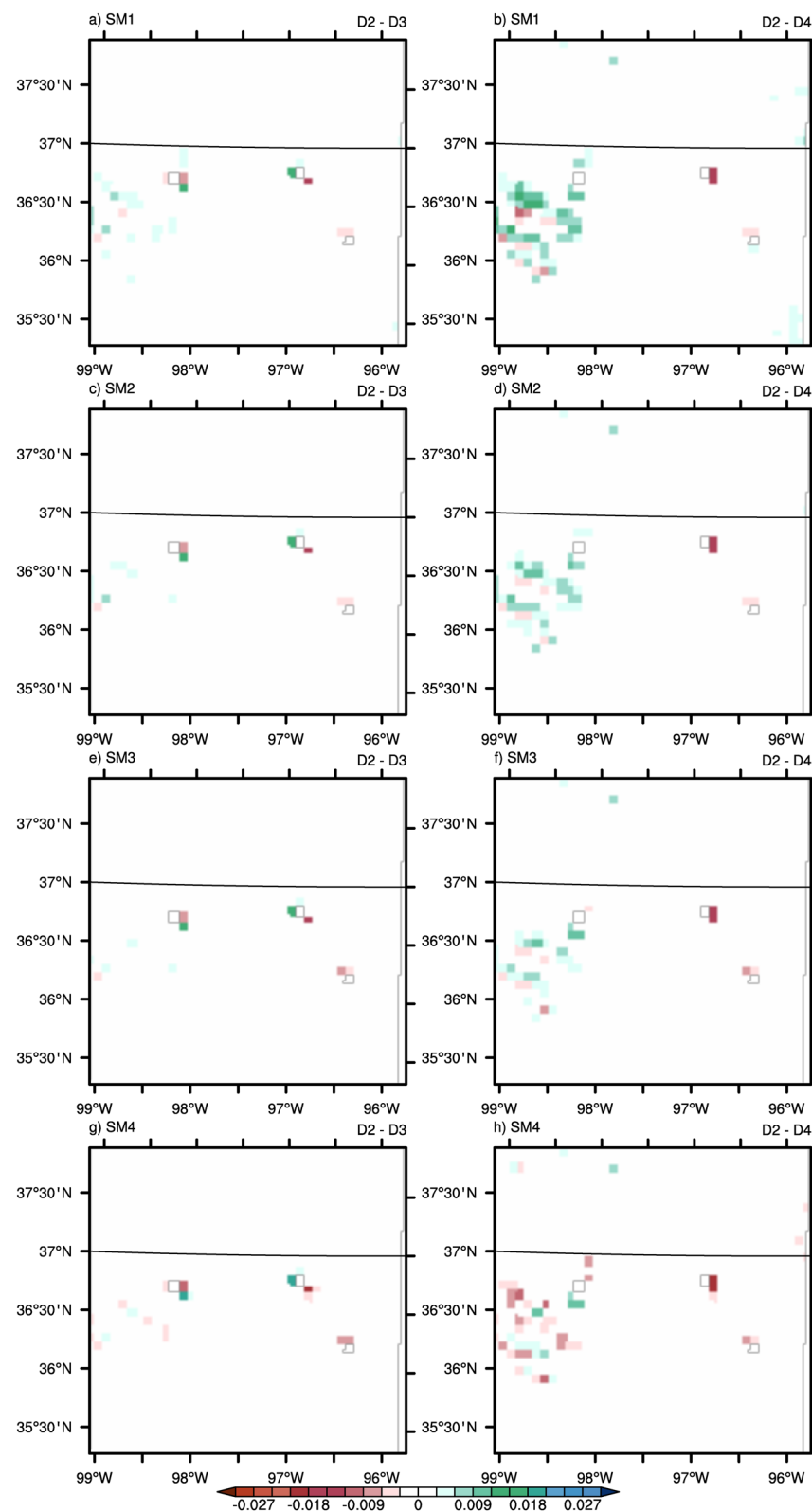


**Figure 12.** Similar as Figure 10, but for land surface model resolution at 10 km.

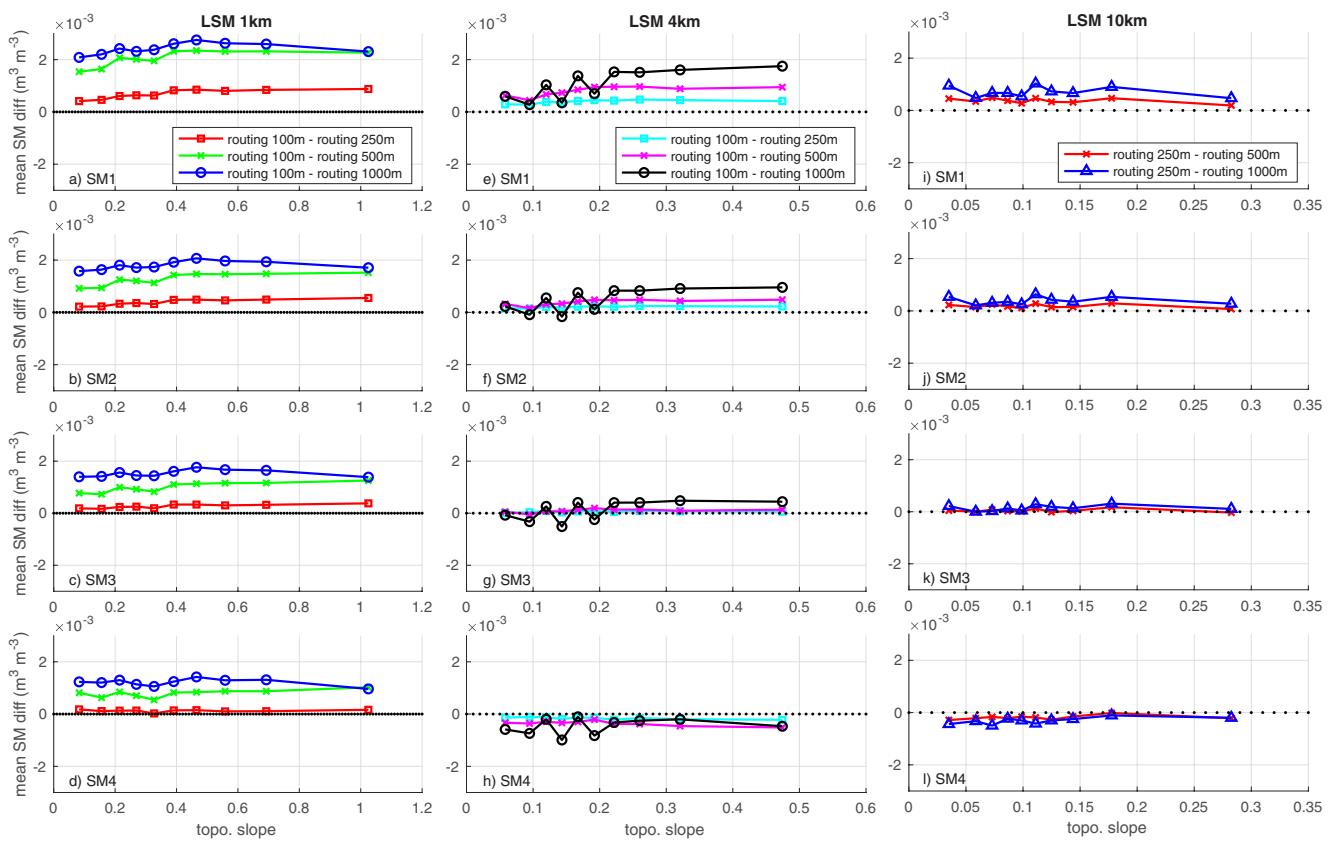


**Figure 13.** Soil moisture difference between different routing resolutions, as a function of slope. (a–d) for land surface model (LSM) at 1 km, (e–h) for LSM at 4 km, and (i–l) for LSM at 10 km.

$$P = ET + \Delta SM + Splus \quad (2)$$

where  $P$  is precipitation (mm),  $ET$  is evapotranspiration (mm),  $\Delta SM$  is the change in soil water content (mm), and  $Splus$  is water surplus. Because there only exists a short lag between the generation of surplus water from precipitation and the resultant streamflow, the water surplus can also be seen as a proxy for runoff (Xue et al., 2018). Figure 14 shows the differences in water balance components for simulations with LSM resolution at 1 km (B2–B5) for JJA 2015. Note that patterns shown in Figure 14 are the differences between the high and low-resolution routing. Precipitation is the same in these experiments, so it is not shown. Figures 14a–14c indicates that there is less soil moisture storage change induced in the high-resolution routing. Since soil moisture is gradually decreasing during the JJA months, suggesting that there is overall more soil moisture in the high-resolution routing, which is consistent with Figure 10. Because of the presence of more soil moisture over the domain,  $ET$  is also more in the high-resolution routing (Figures 14d–14f). Based on the water balance equation (Equation 2), Figures 14g–14i show the difference in Surplus, which can be viewed as the amount of water turned into streamflow in the channel, as explained earlier. It suggests that there is less water converted into streamflow in the high-resolution routing than in the low-resolution routing, which can be attributed to the generation of surface runoff (Figures 14j–14l). Note the similarity in spatial pattern between surface runoff and Surplus. There is more overland surface runoff when routing at high resolution. The amount of overland surface runoff originates as infiltration excess, which is a function of precipitation, existing water head, and infiltration capacity. When calculating lateral surface flow, the effect of terrain slope is taken into account as part of the friction slope. With high routing resolution, the terrain effect is more obvious as terrain slope is not smoothed out as in low-resolution routing. Under the same condition, in high-resolution routing, there will be more surface runoff generated and converged toward lower elevations, and because surface runoff will keep existing on the land surface, unlike being removed after each time step in the default Noah-MP, the existing surface runoff will

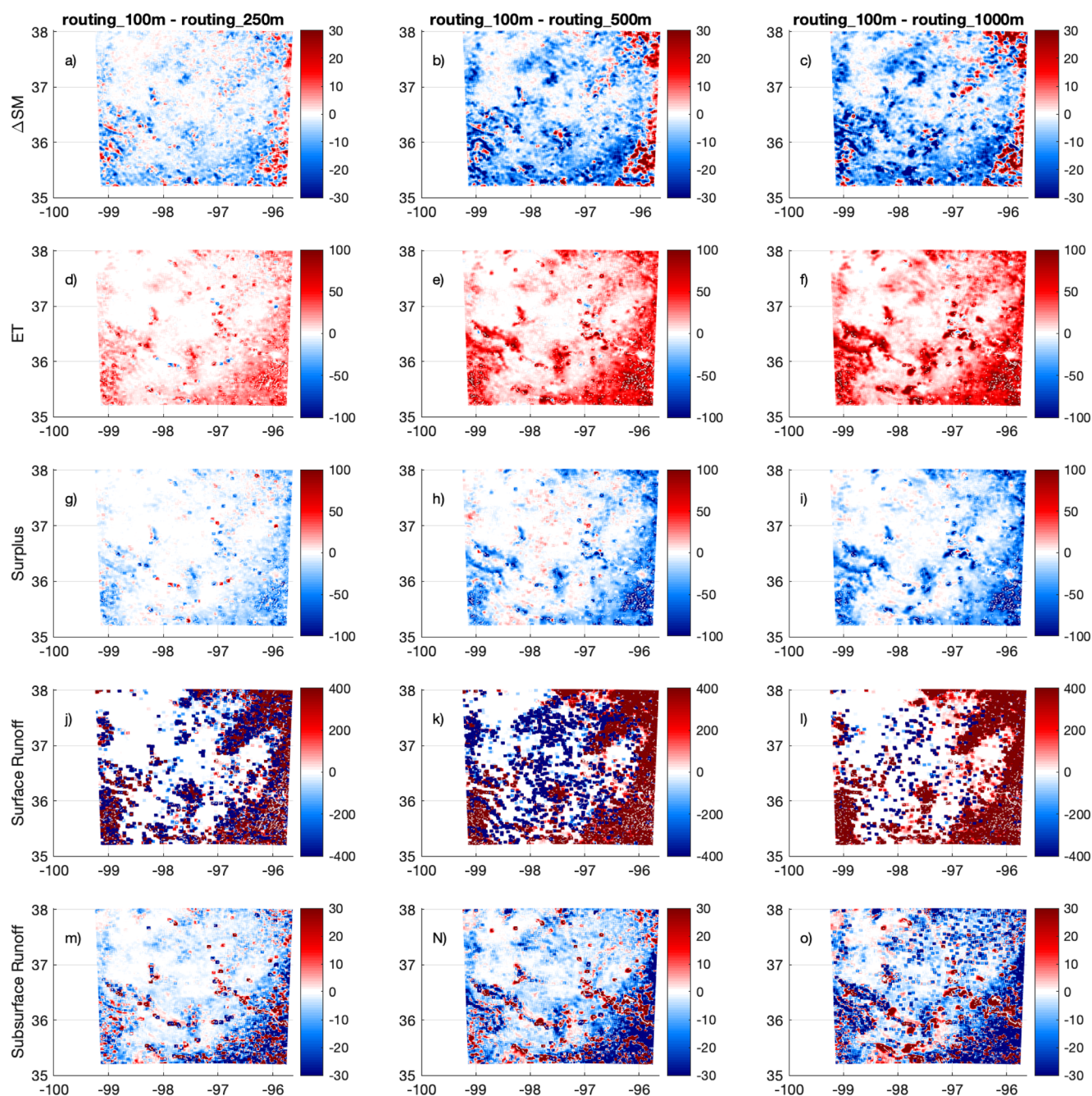


**Figure 14.** Routing-resolution induced differences in water budget components and surface and subsurface runoff. Difference in soil moisture storage term ( $\Delta SM$ ) induced by high and low routing resolution (a) between routing at 100 m and routing at 250 m, (b) between routing 100 m and routing at 500 m, (c) between routing 100 m and routing at 1,000 m. (d–f) are the same as (a–c) but for evapotranspiration (ET). (g–i) are the same as (d–f) but for Surplus water. (j–l) are the same as (d–f) but for surface runoff. (m–o) are the same as (d–f) but for subsurface runoff.

remain in the domain and keep recharging the shallower soil layers, thus increasing ET. This explains the soil moisture and ET differences shown in Figures 10 and Figures 14d–14f. From a water balance perspective, more surface runoff in the high-resolution routing results in less subsurface runoff; this explains the opposite pattern in subsurface runoff seen in Figures 14m–14o. Similar results are found (not shown) for LSM grid spacings of 4 km (C1–C5) and 10 km (D1–D4).

#### 4. Discussion

WRF-Hydro still underestimates latent heat fluxes over the SGP, even when more realistic inputs and boundary forcings are included. As a result, more energy is partitioned into SH, resulting in a warm bias that is a well-known issue in the modeling community. Many studies have attempted to address it from different perspectives (Lin et al., 2017; Ma et al., 2018; Van Weverberg et al., 2018; C. Zhang, Xie, et al., 2018; Y. Zhang, Schaap, & Zha, 2018) and different theories are proposed. For example, an underestimation in evaporative fraction (EF, defined as the ratio of LH to the sum of LH and SH) has been attributed as the dominant source of error in models with a large warming bias. Handling of anthropogenic impacts (or lack thereof), such as neglecting irrigation in the LSMs, has also been attributed to the warming bias (Pei et al., 2016; Qian et al., 2020; Z. Yang et al., 2019). Here, we show that increased LH and decreased SH occur when lateral flow is considered, suggesting that lateral flow might also play an important role in alleviating the warming bias over the SGP.

Comparing simulations using the STATSGO and gSSURGO soil data sets, we found that differences in soil hydraulic parameters are quite large and lead to changes in domain-averaged surface energy fluxes and soil moisture. The use of different soil parameter tables gives us the opportunity to identify which soil parameters are the most sensitive ones to control the rate of energy fluxes and soil moisture. As shown earlier, MAXSMC and SATDK show the strongest control on energy fluxes and MAXSMC and WLTSMC have the strongest impact for soil moisture, which agrees with previous sensitivity studies such as in Cuntz et al. (2016) and Cai et al. (2014).

We note that the baseline Noah-MP model tends to overestimate soil moisture and underestimate LH, which indicates more water should be evaporated into the atmosphere instead of retaining in the soil layers. This bias could potentially be addressed by adjusting parameters suggested in previous parameter sensitivity studies (e.g., Cai et al., 2014; Cuntz et al., 2016; Hogue et al., 2006). For example, the surface dryness factor, which is defined to determine the soil surface resistance to ground evapotranspiration, will increase the soil evaporation as it increases. Similarly, increases in evapotranspiration can also be achieved by lowering the stomatal resistance ( $rsmin$  or  $rcmin$ ) as it determines the diffusion of water from inside the leaf to the atmosphere. Another option is to increase roughness length, as it will affect the intensity of mechanical turbulence and fluxes above the surface. A larger roughness implies more exchange between the surface and the atmosphere. Calibrating these parameters can improve the model performance. However, as stated earlier, the purpose of this study is not on parameter calibration or estimation, but rather on understanding the sensitivity by using different sources of input forcings.

It is also worth stating that LSMs like Noah-MP were originally developed for simulations with much coarser grid spacings (e.g.,  $\sim 25$  km). Some assumptions and parameters used in these models need to be revisited when running at higher resolutions. For instance,  $F_{max}$  is the potential or maximum saturated fraction for a grid cell that was initially derived following the TOPMODEL concepts rooted from watershed hydrology. When high-resolution digital elevation models (DEMs) are available,  $F_{max}$  can be estimated from the distribution function of a logarithmic topographic index that varies spatially and is resolution-dependent (Niu et al., 2011), while in typical coarse resolution applications, it is often set universally as 0.38 for convenience. Another example is the maximum subsurface runoff  $R_{sb,max}$  which should also be spatially varying and resolution dependent but has been set at  $5.0 \times 10^{-4} \text{ mm s}^{-1}$  based on calibration against the global runoff field (Niu et al., 2011). When running at higher resolutions, these hard coded parameters will likely need to be revisited.

We also found that if another soil reference data set is used, that is, the soil water and temperature system (SWATS), the simulated soil moisture is consistently underestimated. The reason we use STAMP instead of SWATS is because STAMP soil moisture is deemed as significantly more reliable than the SWATS (Jenni, 2020, personal communication). Therefore, we recommend taking precautions when choosing reference data sets since they also contain uncertainties that could lead to opposite conclusions.

It is interesting to see that both lateral surface and subsurface flow contribute to increased soil moisture over the SGP. From the water balance perspective, when lateral flow is not turned on, surface runoff is generated when the effective precipitation exceeds the maximum infiltration capacity of the underlying soil column. The calculated surface runoff is then accumulated and removed from the model hydrological budget. At the

next time step, the sum of precipitation rate and existing ponded water head needs to be greater than infiltration capacity again to be able to generate surface runoff. Conversely, when lateral flows are considered, effective precipitation is more likely to accumulate on the grid cell given the existence of ponded water, as long as the sum of precipitation rate and existing ponded water is greater than the infiltration capacity. Therefore, when surface lateral flow is turned on, it is more likely to generate and maintain runoff on the surface. The infiltration excess or ponded water later moves freely in the presence of a hydraulic gradient and infiltrates into the soil column, thereby increasing soil moisture over the domain.

Since the lateral flow process involves the disaggregation-aggregation and routing of surface and subsurface flows, computation costs are significantly increased in the offline WRF-Hydro simulations when lateral flow is turned on. We find that with finer LSM resolution (at 1 km), soil moisture is more sensitive to the choice of routing resolution, especially over steeper terrains. This may shed light on the choice of LSM and routing resolution at different topographic conditions. For example, for complex terrain, one may benefit from high LSM and routing resolution and conversely, over flat regions high-resolution routing may be not necessary, especially when LSM resolution is coarse. One could take advantage of this and design optimized, multi-resolution model grids that only employ high resolution for the LSM and routing where there are larger benefits.

## 5. Conclusions

Using WRF-Hydro, we performed a series of experiments to study the effect of lateral flow on soil moisture and surface energy fluxes over the SGP. To ensure the correctness of input forcing, gSSURGO soil data set, a new soil parameter table, MODIS dynamic vegetation, and Stage-IV precipitation are ingested into the model for the purpose of minimizing uncertainties associated with input forcing, where possible. By switching on and off lateral flow options, and testing different combinations of routing and LSM resolution in the WRF-Hydro, a series of tests were performed to understand their impact on the soil moisture and surface energy fluxes. We summarize our key findings as follows:

- When compared with observations collected at the STAMP sites, the newly developed gSSURGO is found to perform identically as the default STATSGO soil data set, as both soil data sets extracted at the nearest grid cells have 6 out of 16 sites that have the same soil type as the STAMP.
- The default Noah-MP underestimates latent heat fluxes and overestimates soil moisture when compared with observations collected at the ARM sites. Ingesting the updated realistic input forcing does not reduce these biases, which indicates there are deficiencies embedded in the model. Parameter calibration could potentially alleviate such deficiencies (Fersch et al., 2020), but the trend toward higher-resolution modeling primarily suggests to enhance model correspondence to physical reality by representing new processes such as lateral flow in this study, or other processes such as groundwater-surface water interaction, rooting dynamics, and/or irrigation in the model.
- The impact of surface and subsurface lateral flow on soil moisture behaves differently. Surface lateral flow is more likely to increase soil moisture over the lower terrain and convergence zones, without affecting soil moisture over steeper terrain. This is likely induced by the efficient redistribution of water from high to low elevation. The subsurface lateral flow also exhibits an increase in soil moisture over the entire domain, but with a stronger signal over the steep terrain. Subsurface lateral flow increases soil moisture in shallower layers but decreases soil moisture in the deeper layers because of the re-infiltration process, that is, with a sufficiently strong topographic gradient, deep-layer soil moisture is transported to shallower layers at the next downstream grid cells, resulting in the opposite response of soil moisture in the soil column.
- Routing resolution is found to be an important regulator to the response of soil moisture. With high LSM resolutions, the response of soil moisture is very sensitive to the choice of routing resolution and higher soil moisture is seen with finer routing resolution, especially over the steep terrain. With lower LSM resolution, the added value of using high-resolution routing becomes smaller, for example, the difference between routing at 100 and 250 m spacing when LSM grid spacing is 4 km, between routing at 250 and 500 m spacing when LSM grid spacing 10 km, are almost negligible. This indicates that as LSM resolutions get coarser, it is not necessary to use high routing resolution. This indicates that as LSM resolutions get finer, it is necessary to refine routing representations and better estimate their parameters.

Such studies are becoming more critical as weather and climate models are moving into higher and higher resolutions.

The present study focuses primarily on the response of soil moisture and energy fluxes to different input forcing, lateral flow, and LSM and routing resolution. We acknowledge that the calibration of the parameters associated with generating runoff (Fersch et al., 2020; Lahmers et al., 2019, 2020; Yucel et al., 2015; Z. Zhang et al., 2019) is important to ensure reasonable streamflow predictions. It should be noted that the goal of this study is not to calibrate the WRF-Hydro model or obtain a best model configuration with smallest model bias. Instead, our objectives are to quantify the impact of model input, including soil types and properties, precipitation, vegetation and routing processes on simulation results, and to improve our process-level understanding of hydrology in this region. The differences induced by different resolution also calls attention to scale awareness in future development of the routing scheme.

## Conflict of Interest

The authors declare no conflict of interests.

## Data Availability Statement

The WRF-Hydro was downloaded from the NCAR Research Application Laboratory website ([https://ral.ucar.edu/projects/wrf\\_hydro/model-code](https://ral.ucar.edu/projects/wrf_hydro/model-code)). The ArcGIS toolbox for preprocessing the DEM data was accessed at: [https://ral.ucar.edu/projects/wrf\\_hydro/pre-processing-tools](https://ral.ucar.edu/projects/wrf_hydro/pre-processing-tools). All the scripts for generating the figures are available at Zenodo <http://doi.org/10.5281/zenodo.4521316>.

## Acknowledgments

This research was supported by the Office of Science of the U.S. Department of Energy (DOE) as part of the Atmospheric System Research (ASR) Program via grant KP1701000/57131. The research used computational resources from PNNL Research Computing. The Pacific Northwest National Laboratory is operated for DOE by Battelle Memorial Institute under Contract DE-A06-76RLO 1830. The authors appreciate constructive comments that help to improve the manuscript from the anonymous reviewers. The authors thank the developers for providing the NLDAS-2, Stage-IV, and ARM observations.

## References

- Arnault, J., Rummier, T., Baur, F., Lerch, S., Wagner, S., Fersch, B., et al. (2018). Precipitation sensitivity to the uncertainty of terrestrial water flow in WRF-Hydro: An ensemble analysis for Central Europe. *Journal of Hydrometeorology*, 19(6), 1007–1025. <https://doi.org/10.1175/JHM-D-17-0042.1>
- Arnault, J., Wagner, S., Rummier, T., Fersch, B., Bliefernicht, J., Andresen, S., & Kunstmann, H. (2016). Role of runoff-infiltration partitioning and resolved overland flow on land-atmosphere feedbacks: A case study with the WRF-Hydro coupled modeling system for West Africa. *Journal of Hydrometeorology*, 17(5), 1489–1516. <https://doi.org/10.1175/JHM-D-15-0089.1>
- Arnault, J., Wei, J., Rummier, T., Fersch, B., Zhang, Z., Jung, G., et al. (2019). A joint soil-vegetation-atmospheric water tagging procedure with WRF-Hydro: Implementation and application to the case of precipitation partitioning in the Upper Danube River Basin. *Water Resources Research*, 55(7), 6217–6243. <https://doi.org/10.1029/2019WR024780>
- Boussetta, S., Balsamo, G., Beljaars, A., Kral, T., & Jarlan, L. (2013). Impact of a satellite-derived leaf area index monthly climatology in a global numerical weather prediction model. *International Journal of Remote Sensing*, 34(9–10), 3520–3542. <https://doi.org/10.1080/01431612.716543>
- Boussetta, S., Balsamo, G., Dutra, E., Beljaars, A., & Albergel, C. (2014). Analysis of surface albedo and leaf area index from satellite observations and their impact on numerical weather prediction. *ECMWF Technical Memoranda*, 740, 5–10.
- Cai, X., Yang, Z.-L., David, C. H., Niu, G.-Y., & Rodell, M. (2014). Hydrological evaluation of the Noah-MP land surface model for the Mississippi River Basin. *Journal of Geophysical Research: Atmospheres*, 119(1), 23–38. <https://doi.org/10.1002/2013JD020792>
- Chaney, N. W., Metcalfe, P., & Wood, E. F. (2016). HydroBlocks: A field-scale resolving land surface model for application over continental extents. *Hydrological Processes*, 30(20), 3543–3559. <https://doi.org/10.1002/hyp.10891>
- Chen, F., & Dudhia, J. (2001). Coupling an advanced land surface-hydrology model with the Penn State-NCAR MM5 modeling system. Part I: Model implementation and sensitivity. *Monthly Weather Review*, 129(4), 569–585. [https://doi.org/10.1175/1520-0493\(2001\)129<0569:CAALSH>2.0.CO;2](https://doi.org/10.1175/1520-0493(2001)129<0569:CAALSH>2.0.CO;2)
- Clark, M. P., Fan, Y., Lawrence, D. M., Adam, J. C., Bolster, D., Gochis, D. J., et al. (2015). Improving the representation of hydrologic processes in Earth System Models. *Water Resources Research*, 51(8), 5929–5956. <https://doi.org/10.1002/2015WR017096>
- Cosby, B. J., Hornberger, G. M., Clapp, R. B., & Ginn, T. R. (1984). A statistical exploration of the relationships of soil moisture characteristics to the physical properties of soils. *Water Resources Research*, 20(6), 682–690. <https://doi.org/10.1029/WR020i006p00682>
- Cuntz, M., Mai, J., Samaniego, L., Clark, M., Wulfmeyer, V., Branch, O., et al. (2016). The impact of standard and hard-coded parameters on the hydrologic fluxes in the Noah-MP land surface model. *Journal of Geophysical Research: Atmospheres*, 121, 10676–10700. <https://doi.org/10.1002/2016JD025097>
- Daly, C., Halbleib, M., Smith, J. I., Gibson, W. P., Doggett, M. K., Taylor, G. H., et al. (2008). Physiographically sensitive mapping of climatological temperature and precipitation across the conterminous United States. *International Journal of Climatology*, 28(15), 2031–2064. <https://doi.org/10.1002/joc.1688>
- De Lannoy, G. J. M., Koster, R. D., Reichle, R. H., Mahanama, S. P. P., & Liu, Q. (2014). An updated treatment of soil texture and associated hydraulic properties in a global land modeling system. *Journal of Advances in Modeling Earth Systems*, 6(4), 957–979. <https://doi.org/10.1002/2014MS000330>
- Du, J. (2011). *GCIP/EOP surface: Precipitation NCEP/EMC 4KM Gridded Data (GRIB) stage IV data. version 1.0*. UCAR/NCAR—Earth Observing Laboratory. <https://doi.org/10.5065/D6PG1QD4>
- Fan, Y., Clark, M., Lawrence, D. M., Swenson, S., Band, L. E., Brantley, S. L., et al. (2019). Hillslope hydrology in global change research and earth system modeling. *Water Resources Research*, 55(2), 1737–1772. <https://doi.org/10.1029/2018WR023903>

- Fersch, B., Senatore, A., Adler, B., Arnault, J., Mauder, M., Schneider, K., et al. (2020). High-resolution fully coupled atmospheric-hydrological modeling: A cross-compartment regional water and energy cycle evaluation. *Hydrology and Earth System Sciences*, 24(5), 2457–2481. <https://doi.org/10.5194/hess-24-2457-2020>
- Gochis, D. J., Barlage, M., Dugger, A., FitzGerald, K., Karsten, L., McAllister, M., et al. (2018). *The WRF-Hydro modeling system technical description*, (version 5.0) (NCAR Technical Note, p. 107). <https://doi.org/10.5065/D6J38RBJ>. Retrieved from <https://ral.ucar.edu/sites/default/files/public/WRF-HydroV5TechnicalDesc>
- Gochis, D. J., & Chen, F. (2003). *Hydrological enhancements to the community Noah land surface model* (NCAR Technical Note, NCAR/TN-454+STR, p. 68). Retrieved from <http://www.ucar.edu/communications/technotes/>
- Hogue, T. S., Bastidas, L. A., Gupta, H. V., & Sorooshian, S. (2006). Evaluating model performance and parameter behavior for varying levels of land surface model complexity. *Water Resources Research*, 42(8). <https://doi.org/10.1029/2005WR004440>
- Jenni, K. (2020). *Personal communication*.
- Ji, P., Yuan, X., & Liang, X.-Z. (2017). Do lateral flows matter for the hyperresolution land surface modeling? *Journal of Geophysical Research: Atmospheres*, 122(22), 12077–12092. <https://doi.org/10.1002/2017JD027366>
- Jordan, R. E. (1991). *A one-dimensional temperature model for a snow cover*. Technical documentation for SNTHERM.89. Cold Region Research and Engineering Laboratory, U.S. Army Corps of Engineers.
- Julien, P. Y., Saghafian, B., & Ogden, F. L. (1995). Raster-based hydrologic modeling of spatially-varied surface runoff. *Journal of the American Water Resources Association*, 31(3), 523–536. <https://doi.org/10.1111/j.1752-1688.1995.tb04039.x>
- Kishné, A. S., Yimam, Y. T., Morgan, C. L. S., & Dornblaser, B. C. (2017). Evaluation and improvement of the default soil hydraulic parameters for the Noah Land Surface Model. *Geoderma*, 285(C), 247–259. <https://doi.org/10.1016/j.geoderma.2016.09.022>
- Knote, C., Bonafe, G., & Di Giuseppe, F. (2009). Leaf area index specification for use in mesoscale weather prediction systems. *Monthly Weather Review*, 137(10), 3535–3550. <https://doi.org/10.1175/2009mwr2891.1>
- Koster, R. D., Dirmeyer, P. A., Guo, Z., Bonan, G., Chan, E., Cox, P., et al. (2004). Regions of strong coupling between soil moisture and precipitation. *Science*, 305(5687), 1138–1140. <https://doi.org/10.1126/science.1100217>
- Kumar, A., Chen, F., Barlage, M., Ek, M. B., & Niyogi, D. (2014). Assessing impacts of integrating MODIS vegetation data in the Weather Research and Forecasting (WRF) Model coupled to two different canopy-resistance approaches. *Journal of Applied Meteorology and Climatology*, 53(6), 1362–1380. <https://doi.org/10.1175/JAMC-D-13-0247.1>
- Lahmers, T. M., Castro, C. L., & Hazenberg, P. (2020). Effects of lateral flow on the convective environment in a coupled hydrometeorological modeling system in a semiarid environment. *Journal of Hydrometeorology*, 21(4), 615–642. <https://doi.org/10.1175/JHM-D-19-0100.1>
- Lahmers, T. M., Gupta, H., Castro, C. L., Gochis, D. J., Yates, D., Dugger, A., et al. (2019). Enhancing the structure of the WRF-Hydro hydrologic model for semiarid environments. *Journal of Hydrometeorology*, 20(4), 691–714. <https://doi.org/10.1175/JHM-D-18-0064.1>
- Lin, Y., Dong, W., Zhang, M., Xie, Y., Xue, W., Huang, J., & Luo, Y. (2017). Causes of model dry and warm bias over central U.S. and impact on climate projections. *Nature Communications*, 8(1), 1–8. <https://doi.org/10.1038/s41467-017-01040-2>
- Livneh, B., Kumar, R., & Samaniego, L. (2015). Influence of soil textural properties on hydrologic fluxes in the Mississippi River basin. *Hydrological Processes*, 29(21), 4638–4655. <https://doi.org/10.1002/hyp.10601>
- Ma, H. Y., Klein, S. A., Xie, S., Zhang, C., Tang, S., Tang, Q., et al. (2018). CAUSES: On the role of surface energy budget errors to the warm surface air temperature error over the Central United States. *Journal of Geophysical Research: Atmospheres*, 123(5), 2888–2909. <https://doi.org/10.1002/2017JD027194>
- Mather, J. R. (1978). *The climatic water budget in environmental analysis*. Free Press. <https://doi.org/10.1007/978-1-4613-3387-6>
- Maxwell, R. M., Condon, L. E., & Kollet, S. J. (2015). A high-resolution simulation of groundwater and surface water over most of the continental US with the integrated hydrologic model ParFlow v3. *Geoscientific Model Development*, 8(3), 923–937. <https://doi.org/10.5194/gmd-8-923-2015>
- McKay, L., Bondelid, T., Dewald, T., Johnston, J., Moore, R., & Rea, A. (2012). *NHDPlus version 2: User guide*. <https://doi.org/10.2316/p.2012.774-048>
- Miller, D. A., & White, R. A. (1998). A conterminous United States multilayer soil characteristics dataset for regional climate and hydrology modeling. *Earth Interactions*, 2, 1–26. [https://doi.org/10.1175/1087-3562\(1998\)002<0001:ACUSMS>2.3.CO;2](https://doi.org/10.1175/1087-3562(1998)002<0001:ACUSMS>2.3.CO;2)
- Morcrette, C. J., Van Weverberg, K., Ma, H. Y., Ahlgrimm, M., Bazile, E., Berg, L. K., et al. (2018). Introduction to CAUSES: Description of weather and climate models and their near-surface temperature errors in 5 day hindcasts near the southern Great Plains. *Journal of Geophysical Research: Atmospheres*, 123, 2655–2683. <https://doi.org/10.1002/2017jd027199>
- Mynden, R., Knyazikhin, Y., & Park, T. (2015). MYD15A2H MODIS/aqua leaf area index/FPAR 8-day L4 global 500m SIN grid V006 (Data set). NASA EOSDIS Land Processes DAAC. <https://doi.org/10.5067/MODIS/MYD15A2H.006>
- NCEP. (2012). *Module SF NOAH-LSM v. 3.4.1*. Retrieved from [http://www.ral.ucar.edu/research/land/technology/lsm/noahlsms-v3.4.1/modulsf\\_noahlsms.F](http://www.ral.ucar.edu/research/land/technology/lsm/noahlsms-v3.4.1/modulsf_noahlsms.F)
- Niu, G.-Y., Yang, Z.-L., Mitchell, K. E., Chen, F., Ek, M. B., Barlage, M., et al. (2011). The community Noah land surface model with multiparameterization options (Noah-MP): 1. Model description and evaluation with local-scale measurements. *Journal of Geophysical Research*, 116(D12). <https://doi.org/10.1029/2010JD015139>
- Ogden, F. L. (1997). *CASC2D reference manual* (p. 106). Department of Civil and Environmental Engineering, University of Connecticut.
- Osborne, T. M., Lawrence, D. M., Slingo, J. M., Challinor, A. J., & Wheeler, T. R. (2004). Influence of vegetation on the local climate and hydrology in the tropics: Sensitivity to soil parameters. *Climate Dynamics*, 23(1), 45–61. <https://doi.org/10.1007/s00382-004-0421-1>
- Pei, L., Moore, N., Zhong, S., Kendall, A. D., Gao, Z., & Hyndman, D. W. (2016). Effects of irrigation on summer precipitation over the United States. *Journal of Climate*, 29(10), 3541–3558. <https://doi.org/10.1175/JCLI-D-15-0337.1>
- Peters-Lidard, C. D., Blackburn, E., Liang, X., & Wood, E. F. (1998). The effect of soil thermal conductivity parameterization on surface energy fluxes and temperatures. *Journal of the Atmospheric Sciences*, 55(7), 1209–1224. [https://doi.org/10.1175/1520-0469\(1998\)055<1209:TEOSTC>2.0.CO;2](https://doi.org/10.1175/1520-0469(1998)055<1209:TEOSTC>2.0.CO;2)
- Qian, Y., Yang, Z., Feng, Z., Liu, Y., Gustafson, W. I., Berg, L. K., et al. (2020). Neglecting irrigation contributes to climate model summertime warm-and-dry biases in the central United States. *npj Climate and Atmospheric Science*, 3, 31.
- Rummel, T., Arnault, J., Gochis, D., & Kunstmann, H. (2019). Role of lateral terrestrial water flow on the regional water cycle in a complex terrain region: Investigation with a fully coupled model system. *Journal of Geophysical Research: Atmospheres*, 124(2), 507–529. <https://doi.org/10.1029/2018JD029004>
- Sakaguchi, K., & Zeng, X. (2009). Effects of soil wetness, plant litter, and under-canopy atmospheric stability on ground evaporation in the Community Land Model (CLM3.5). *Journal of Geophysical Research*, 114, D01107. <https://doi.org/10.1029/2008JD010834>

- Senatore, A., Mendicino, G., Gochis, D. J., Yu, W., Yates, D. N., & Kunstmann, H. (2015). Fully coupled atmosphere-hydrology simulations for the central Mediterranean: Impact of enhanced hydrological parameterization for short and long time scales. *Journal of Advances in Modeling Earth Systems*, 7(4), 1693–1715. <https://doi.org/10.1002/2015MS000510>
- Shi, Y., Davis, K. J., Zhang, F., & Duffy, C. J. (2014). Evaluation of the parameter sensitivities of a coupled land surface hydrologic model at a critical zone observatory. *Journal of Hydrometeorology*, 15(1), 279–299. <https://doi.org/10.1175/JHM-D-12-0177.1>
- Thornthwaite, C. W. (1948). An approach toward a rational classification of climate. *Geographical Review*, 38(1), 55–94. <https://doi.org/10.2307/210739>
- Van Weverberg, K., Morcrette, C. J., Petch, J., Klein, S. A., Ma, H. Y., Zhang, C., et al. (2018). CAUSES: Attribution of surface radiation biases in NWP and climate models near the U.S. southern Great Plains. *Journal of Geophysical Research: Atmospheres*, 123, 3612–3644. <https://doi.org/10.1002/2017jd027188>
- Wigmsta, M. S., & Lettenmaier, D. P. (1999). A comparison of simplified methods for routing topographically driven subsurface flow. *Water Resources Research*, 35(1), 255–264. <https://doi.org/10.1029/1998WR900017>
- Wigmsta, M. S., Vail, L. W., & Lettenmaier, D. P. (1994). A distributed hydrology-vegetation model for complex terrain. *Water Resources Research*, 30(6), 1665–1679. <https://doi.org/10.1029/94WR00436>
- Wood, E. F., Roundy, J. K., Troy, T. J., van Beek, L. P. H., Bierkens, M. F. P., Blyth, E., et al. (2011). Hyperresolution global land surface modeling: Meeting a grand challenge for monitoring Earth's terrestrial water. *Water Resources Research*, 47(5), 54–10. <https://doi.org/10.1029/2010WR010090>
- Xia, Y., Mitchell, K., Ek, M., Sheffield, J., Cosgrove, B., Wood, E., et al. (2012). Continental-scale water and energy flux analysis and validation for the North American Land Data Assimilation System project phase 2 (NLDAS-2): 1. Intercomparison and application of model products. *Journal of Geophysical Research*, 117, D03109. <https://doi.org/10.1029/2011JD016048>
- Xue, Z., Gochis, D., Yu, W., Keim, B., Rohli, R., Zang, Z., et al. (2018). Modeling hydroclimatic change in southwest Louisiana rivers. *Water*, 10(5), 596. <https://doi.org/10.3390/w10050596>
- Yang, Z., Qian, Y., Liu, Y., Berg, L. K., Hu, H., Dominguez, F., et al. (2019). Irrigation impact on water and energy cycle during dry years over the United States using convection-permitting WRF and a Dynamical Recycling Model. *Journal of Geophysical Research: Atmospheres*, 124(21), 11220–11241. <https://doi.org/10.1029/2019JD030524>
- Yang, Z.-L., Niu, G.-Y., Mitchell, K. E., Chen, F., Ek, M. B., Barlage, M., et al. (2011). The community Noah land surface model with multiparameterization options (Noah-MP): 2. Evaluation over global river basins. *Journal of Geophysical Research*, 116(D12), 4257. <https://doi.org/10.1029/2010JD015140>
- Yucel, I., Onen, A., Yilmaz, K. K., & Gochis, D. J. (2015). Calibration and evaluation of a flood forecasting system: Utility of numerical weather prediction model, data assimilation and satellite-based rainfall. *Journal of Hydrology*, 523(C), 49–66. <https://doi.org/10.1016/j.jhydrol.2015.01.042>
- Zhang, C., Xie, S., Klein, S. A., Ma, H. y., Tang, S., Van Weverberg, K., et al. (2018). CAUSES: Diagnosis of the summertime warm bias in CMIP5 Climate Models at the ARM southern Great Plains site. *Journal of Geophysical Research: Atmospheres*, 123(6), 2968–2992. <https://doi.org/10.1002/2017JD027200>
- Zhang, Y., Schaap, M. G., & Zha, Y. (2018). A high-resolution global map of soil hydraulic properties produced by a hierarchical parameterization of a physically based Water Retention Model. *Water Resources Research*, 54(12), 9774–9790. <https://doi.org/10.1029/2018WR023539>
- Zhang, Z., Arnault, J., Wagner, S., Laux, P., & Kunstmann, H. (2019). Impact of lateral terrestrial water flow on land-atmosphere interactions in the Heihe River Basin in China: Fully coupled modeling and precipitation recycling analysis. *Journal of Geophysical Research: Atmospheres*, 124(5), 8401–8423. <https://doi.org/10.1029/2018JD030174>